

## A RESOLUTION OF THE COSMIC LITHIUM PROBLEM

Rachid Ouyed<sup>1</sup>

*Draft version: September 16, 2021*

### RESUMEN

### ABSTRACT

In 1982, Monique and François Spite discovered that the  ${}^7\text{Li}$  abundance in the atmosphere of old metal-poor dwarf stars in the galactic halo was independent of metallicity and temperature. Since then,  ${}^7\text{Li}$  abundance in the Universe has become a subject of intrigue, because there is less of it in Population II dwarf stars (by a factor of 3) than standard big bang nucleosynthesis predicts. Here we show how quark-novae (QNe) occurring in the wake of Pop. III stars, can elegantly produce an  $A(\text{Li}) \sim 2.2$  Lithium plateau in Pop. II (low-mass) stars formed in the pristine cloud swept up by the mixed SN+QN ejecta. We also find an increase in the scatter as well as an eventual drop in  $A(\text{Li})$  below the Spite plateau values for very low metallicity ( $[\text{Fe}/\text{H}] < -3$ ) in excellent agreement with observations. We propose a solution to the discrepancy between the Big Bang Nucleosynthesis  ${}^7\text{Li}$  abundance and the Spite plateau and list some implications and predictions of our model.

*Key Words:* Cosmology: Early Universe — Cosmology: Abundances — Stars: Population II — Stars: Population III — Supernovae: General

### 1. INTRODUCTION

In 1982, Monique and François Spite made a very important discovery. They found that the abundance of  ${}^7\text{Li}$  is essentially constant in warm metal poor stars in the galactic halo. Their derived abundance shows a plateau with a constant  $A(\text{Li}) \sim 2.2^2$  for effective stellar temperatures of  $5900 \text{ K} < T_{\text{eff}} < 6300 \text{ K}$ . This  $T_{\text{eff}}$  range stands for a metallicity of  $-2.8 < [\text{Fe}/\text{H}] < -2$ . The scatter in  ${}^7\text{Li}$  abundance in these stars is really small, in the order of  $\sim 0.05$  dex e.g. (e.g. Asplund et al. 2006).

Although  ${}^7\text{Li}$  is fragile to a relatively low temperature (e.g.  $T \geq 2.5 \times 10^6 \text{ K}$ ), warm, metal-poor stars (e.g. stars with temperatures of  $T_{\text{eff}} \geq 5900 \text{ K}$ ) have shallow convection zones, which prevents the destruction of  ${}^7\text{Li}$ . The star's atmosphere is not hot enough to destroy  ${}^7\text{Li}$ . If the convection zone is shallow,  ${}^7\text{Li}$  is preserved because it stays in the atmosphere and is not transported to the deeper, hot layers where it could get slowly destroyed<sup>3</sup>. The  ${}^7\text{Li}$  abundance in the atmosphere of these stars is expected to reflect the  ${}^7\text{Li}$  abundance of primitive Galactic matter. In these stars is “tattooed” the chemical composition of the interstellar medium or cloud where they formed.

<sup>1</sup>Department of Physics & Astronomy, University of Calgary, Canada

<sup>2</sup>We adopt the standard definition  $[A/B] = \log(N_A/N_B) - \log(N_A/N_B)_\odot$  and  $A(\text{Li}) = \log(N_{7\text{Li}}/N_{\text{H}}) + 12$ .

<sup>3</sup>In standard stellar models, the expected depletion of  ${}^7\text{Li}$  for metal-poor turnoff stars is negligible, i.e., less than 0.02 dex (Deliyannis et al. 1990; Pinsonneault et al. 1992).

Originally, researchers proposed that this lithium plateau is the  ${}^7\text{Li}$  produced in the Big Bang, i.e. in primordial nucleosynthesis. However, theoretical and observational results challenge the idea (e.g. Ryan et al. 1999; Cyburt et al. 2008). Through the Wilkinson Microwave Anisotropy Probe (WMAP) measurements of the cosmological constants, astronomers now know the abundances of BBN elements ( ${}^3\text{He}$ ,  ${}^4\text{He}$ , D,  ${}^6\text{Li}$  and  ${}^7\text{Li}$ ) produced by the Big Bang. All Big Bang Nucleosynthesis (BBN) elements were observed in the amounts predicted, except for  ${}^7\text{Li}$ . The corresponding primordial  ${}^7\text{Li}$  abundance derived is  $A(\text{Li}) = 2.72^{+0.05}_{-0.06}$  (Cyburt et al. 2008; Coc & Vangioni 2010), which is three times higher than the  ${}^7\text{Li}$  abundance observed in warm low-mass halo stars.

Astronomers have discussed several ways to solve the discrepancy between the Spite plateau and the WMAP/BBN results. One idea involves the destruction of BBN  ${}^7\text{Li}$  through nuclear burning. Primordial, Population III stars deplete BBN lithium through nuclear burning, which leaves a lower lithium abundance that is eventually accreted into Spite plateau stars. However, it appears that this idea cannot explain the entire BBN/Spite plateau gap (e.g. Sbordone et al. 2010). Furthermore, it appeals to Population III stars of 10-40 $M_{\odot}$  which produce a larger yield of CNO elements than the observed abundances in metal-poor halo star (Prantzos 2007).

Another resolution for the Spite/BBN discrepancy involves non-standard BBN models (e.g. Jedamzik et al. 2006; Coc et al. 2009; Iocco et al. 2009; Jedamzik & Pospelov 2009; Kohri & Santoso 2009). These models consider the decay of supersymmetric particles to lower the primordial prediction (e.g. Cyburt et al. 2010). For example, if the late decaying particle is a gravitino, then the Spite plateau may be reconciled with BBN values (e.g. Jedamzik et al. 2006). Yet, these non-standard models cannot explain the dependence of  $A(\text{Li})$  on metallicity below  $[\text{Fe}/\text{H}] \sim -2.8$ .

A third solution involves the modification of reaction cross-sections for the production of  ${}^7\text{Li}$  in BBN (e.g. Chakraborty, Fields & Olive 2011). However, ideas that involve the change of reaction -cross sections for  ${}^7\text{Li}$  were ruled out by nuclear and particle physics (e.g. Coc et al. 2010). Furthermore, large errors in the cross section of the reaction leading to  ${}^7\text{Li}$  are unlikely (e.g. Cyburt et al. 2004; Angulo et al. 2005).

Finally, another idea involves the destruction of BBN lithium through its diffusion into a star's photosphere. Diffusion causes  ${}^7\text{Li}$  (and other elements) to sink below the photosphere where it is destroyed at  $T \geq 2 \times 10^6$  K by reactions with protons (e.g., Michaud et al. 1984; Salaris & Weiss 2001). This depletion could in principle, attenuate the discrepancy between BBN and observed  ${}^7\text{Li}$ . The degree of this photospheric depletion can be parameterized by including mixing in the model (e.g. Lambert 2004). Modellers have applied mixing in diffusion through gravity waves (Talon et al. 2002; Charbonnel & Talon 2005), rotation (e.g., Vauclair 1988; Chaboyer & Demarque 1994; Pinsonneault et al. 2002; Talon & Charbonnel 2004), and turbulence (Richard et al. 2005; Piau 2008). Richard et al. (2005) managed to produce a flat  ${}^7\text{Li}$  abundance along the Spite plateau through a specific parameterization of turbulent mixing.

### 1.1. *The challenge*

Any new model must face the following key issues (see discussion in Spite et al. 2012 and references in Fields 2011): (i) There is a very low scatter in the  ${}^7\text{Li}$  abundances among the Spite plateau stars.  ${}^7\text{Li}$  depletion models face challenges when attempting to reproduce this very low scatter ( $\leq 0.05$  dex); (ii) The meltdown of the Spite plateau is established, but its cause is unclear (Sbordone et al. 2010). Any successful model for the Spite plateau must be able to produce a constant lithium abundance among warm, metal-poor stars with  $[\text{Fe}/\text{H}] > -2.8$  that is metallicity independent and with low scatter. Furthermore, the model must be able to explain the metallicity dependent, high scatter lithium abundance in warm, metal poor stars with  $[\text{Fe}/\text{H}] < -2.8$  as well.

In this paper, we suggest an alternative solution. We argue that the Spite plateau might actually be produced by Quark-Novae (QN). The QN is an evolutionary channel that is triggered after a type II supernova (SNII), where the neutron star (NS) left behind, if massive enough, experiences an explosive phase transition into a quark star (Ouyed et al. 2002; Vogt et al. 2004; Ouyed et al. 2005; Keränen et al. 2005; Niebergal et al. 2010). The explosion releases the neutron-rich outer layers of the parent NS, and these relativistic layers subsequently interact with the ejecta of the prior SNII explosion. This neutron-rich ejecta expands away from the quark star (the compact remnant) at relativistic speeds with an average Lorentz factor  $\Gamma_{\text{QN}} \simeq 10$ ; i.e. a typical neutron energy  $E_{\text{QN}} = 10$  GeV (Keränen et al. 2005; Ouyed et al. 2005).

This interaction causes spallation reactions that produce new, daughter nuclei. In the case of the Spite plateau, we apply the QN model to Population III stars. SNII explosions of Pop. III stars in the  $20M_{\odot} < M < 40M_{\odot}$  range should lead to massive NSs that evolve into QNe. The QN's neutron-rich ejecta spall  ${}^{56}\text{Ni}$  and other SNII isotopes, which produces  ${}^7\text{Li}$  and other daughter nuclei. The fragmentation/destruction of  ${}^{56}\text{Ni}$  leads to iron-impoverishment in the cloud swept up by the combined SN+QN ejecta. These iron-poor clouds form into low metallicity Pop. II stars (Ouyed 2013). A key parameter is the time delay between the first SN explosion and the subsequent QN explosion. The metallicity is a function of  $t_{\text{delay}}$ , where a low  $t_{\text{delay}}$  leads to a higher depletion of  ${}^{56}\text{Ni}$  and therefore a lower metallicity, and a high  $t_{\text{delay}}$  leads to a higher metallicity. We show that this primordial QN can lead to a production of a plateau of  $A(\text{Li}) \sim 2.2$  and satisfy the criteria of low-scatter and appropriate meltdown.

The paper is organized as follows. In section 2, we briefly present the QN model. We explain the basic physics of the QN and discuss it in the context of Pop. III stars. Section 3 describes our model's parameters and how it relates to  ${}^{56}\text{Ni}$  destruction by neutron spallation and the resulting Fe impoverishment. In section 3, we also discuss how spallation results into sub-Fe nuclei and  $\alpha$  elements, and compare this findings to observations. Section 4 describes how our QN model produces  ${}^7\text{Li}$  and a low scatter, plateau of  $A(\text{Li}) \sim 2.2$ . Section 5 discusses our results and predictions. We conclude in Section 6.

## 2. PRIMORDIAL QUARK-NOVAE

The basic picture of the QN is that a massive NS (with  $M_{\text{NS}} > 1.6M_{\odot}$ ) converts explosively to a quark star. Such an explosion can happen if the massive NS, in its spin-down evolution or via mass accretion (e.g. from fall-back material), reaches the quark de-confinement density in its core (Staff et al. 2006) and subsequently undergoes a phase transition to the conjectured more stable strange quark matter phase (Itoh 1970; Bodmer 1971; Witten 1984; see also Terazawa 1979). This results in a strange quark matter conversion front that propagates toward the surface of the NS with a detonation occurring before the surface is reached (Keränen et al. 2005; Niebergal et al. 2010). The outcome of the QN explosion – besides the formation of a quark star – is the ejection of the NS’s outermost layers (a very neutron-rich ejecta with an average mass  $M_{\text{QN}} \sim 10^{-3}M_{\odot}$ ) at relativistic speeds (with a Lorentz factor averaging  $\Gamma_{\text{QN}} \sim 10$ ; the evolution of this ejecta was analysed in details in Ouyed&Leahy 2009). The outer layers are ejected from an expanding thermal fireball (Vogt et al. 2004; Ouyed et al. 2005) which allows for ejecta with kinetic energy,  $E_{\text{QN}}^{\text{KE}} > 10^{52}$  erg. Hereafter we assume that a typical neutron in the QN ejecta will be streaming out with energy  $E_{\text{QN}} \simeq 10$  GeV; not to be confused with the total ejecta’s kinetic energy  $E_{\text{QN}}^{\text{KE}}$ . This means that the  $M_{\text{QN}} \sim 10^{-3}M_{\odot}$  QN ejecta will have a typical total kinetic energy of  $E_{\text{QN}}^{\text{KE}} \sim 2 \times 10^{52}$  erg.

### 2.1. Dual-shock Quark Novae (dsQNe)

When the QN occurs a few days to a few weeks following the preceding Type II SN (SNII) explosion, a dual-shock QN (hereafter dsQNe) is created. The interaction between the relativistic, neutron-rich, QN ejecta and the SNII ejecta leads to spallation of the SN material (Ouyed et al. 2011). This time delay,  $t_{\text{delay}}$ , plays a crucial role in our model since it defines the density of the expanding SN ejecta (and thus spallation efficiency) when it is hit by the  $E_{\text{QN}} \sim 10$  GeV QN neutrons (the primaries in our model; see §3.1 below). If the time  $t_{\text{delay}}$  between SN and QN explosions is too lengthy (of the order of months), the SN ejecta will have dissipated such that the QN erupts in isolation. However, when  $t_{\text{delay}}$  is on the order of days to weeks the neutron-rich QN ejecta interacts with the preceding SN ejecta leading to spallation products that are unique to dsQNe (Ouyed et al. 2011; Ouyed 2013).

### 2.2. The Pop. III Type-II SN (PopIII-SNII) progenitor

Studies of star formation in the early Universe suggest that the first stars (Pop. III) were more massive than present day objects, with a typical mass of  $\sim 100M_{\odot}$  for zero metallicity ( $Z$ ) objects (Abel et al. 2002; Nakamura & Umemura 2002; Bromm&Larson 2004; Loeb et al. 2008). The progenitors of QNe are stars with masses in the  $20M_{\odot} < M_{\text{prog.}} < 40M_{\odot}$  range (e.g. Ouyed et al. 2009a; Ouyed et al. 2009b; Leahy&Ouyed 2009; Ouyed&Leahy 2013; Ouyed 2013). Thus, primordial QNe are expected to occur in the wake of these Pop. III stars from progenitors with mass range at the lower end of the mass distribution. These are expected to explode as TypeII SNe and would most likely form NSs massive enough to result in QNe once quark de-confinement density is reached in their cores (Staff et al. 2006). Hereafter we refer to them as PopIII-SNII progenitors.

### 3. OUR MODEL

In this section, we summarize and discuss our model's parameters and its general features and present some results. As in our previous studies, in all of the calculations presented here, we divide the target layer into  $N_{\text{mfp},A_T}$  sublayers of radial thickness equivalent to a spallation mean-free-path (mfp),  $\lambda_{\text{sp},A_T}$ . In each mfp of interaction, a given nucleus with atomic number  $A_T$  will be hit multiple times by the neutrons. To produce a realistic distribution of product nuclei from this sub-layer, we draw the number of hits from a Poisson distribution. The interested reader is referred to Ouyed et al. (2011; see eqs 3, 4 and 5 in that paper) and Ouyed (2013) for more details on the spallation process, numerical procedure, and relevant references.

#### 3.1. Model Parameters

We start by summarizing the key parameters in our model:

- The PopIII-SNII ejecta's composition:** Studies of the chemical composition of PopIII-SNII ejecta in the  $20M_\odot < M_{\text{prog.}} < 40M_\odot$  mass range can be found in the literature for mixed and unmixed SN ejecta (Umeda&Nomoto 2002; Nozawa et al. 2003; Cherchneff&Dwek 2009; Heger& Woosley 2010). Among the main products of these PopIII-SNII supernovae as listed in these studies are  $^{56}\text{Ni}$ ,  $^{32}\text{S}$ ,  $^{28}\text{Si}$ ,  $^{24}\text{Mg}$ ,  $^{20}\text{Ne}$ ,  $^{16}\text{O}$  and,  $^{12}\text{C}$ . Other elements (including  $^{14}\text{N}$ ; see §3.3 below) are present at much smaller levels so we ignore them here. We also ignore elements heavier than  $^{56}\text{Ni}$  in the present study. While some differences exist in mass yields arrived by different studies/groups, and between models with mixing and non-mixing, we find that a typical  $20M_\odot$  PopIII-SN ejecta (with  $10^{51}$  erg in energy) can be represented with an averaged mass yields of  $M_{\text{Ni,SN}} \sim 0.1M_\odot$ ,  $M_{\text{S,SN}} \sim 0.05M_\odot$ ,  $M_{\text{Si,SN}} \sim 0.05M_\odot$ ,  $M_{\text{Mg,SN}} \sim 0.05M_\odot$ ,  $M_{\text{Ne,SN}} \sim 0.05M_\odot$ ,  $M_{\text{O,SN}} \sim 1.5M_\odot$ ,  $M_{\text{C,SN}} \sim 0.15M_\odot$ . We adopt these values as initial, fiducial, values for the target material; i.e. the PopIII-SN ejecta in our model.

Although some mixing is likely to occur during the PopIII-SNII explosions, here we assume an onion-like profile of the expanding SN ejecta (i.e., no mixing) with the innermost ejecta, viz.,  $^{56}\text{Ni}$  nuclei (mass number  $A_T=56$ ) constituting the target  $A_T$  at a distance  $R_{A_T}(t_{\text{delay}})=v_{\text{sn}} t_{\text{delay}}$  from the center of the explosion. Furthermore, we point out that we assume  $v_{\text{sn}}$  to be constant since the QN occurs while the SN ejecta is still in the Sedov phase (e.g., McCray 1985). Carbon ( $^{12}\text{C}$ ) makes up the last layer in this onion-like geometry overlaying the Oxygen layer. The  $^4\text{He}$  and H layers overlaying the carbon layer can be ignored since in most cases considered here we find that the spallation mean-free-path of the (primary, secondary and subsequent generations of) neutrons always exceeds the (H and  $^4\text{He}$ ) layers' thickness.

- The time delay ( $t_{\text{delay}}$ ):** The number density in the target layer (made of element with atomic number  $A_T$ ) for the case of a uniform density is  $n_{A_T} = M_{A_T,\text{SN}}/(4\pi R_{A_T}^2 \Delta R_{A_T} A_T m_{\text{H}})$  where  $M_{A_T,\text{SN}}$  is the mass of the layer (the target's initial mass in the PopIII-SN ejecta prior to impact by the QN neutrons),

$\Delta R_{A_T}$  the layer's thickness and  $R_{A_T} = v_{\text{sn}} t_{\text{delay}}$  the radius of the layer from the center of the SN explosion;  $m_H$  is the hydrogen mass. For a given PopIII-SNII explosion with known  $M_{A_T, \text{SN}}$  (e.g. for a fixed amount of  $^{56}\text{Ni}$  processed during the explosion) and given  $v_{\text{sn}}$ , which we assume to remain constant early in the expansion of the SN ejecta,  $t_{\text{delay}}$  becomes the key parameter that defines the target density. In this prescription, the longer the time delay,  $t_{\text{delay}}$ , the lower the target density when it is hit by the relativistic QN neutrons.

The neutron spallation mfp on a target  $A_T$  is  $\lambda_{\text{sp}, A_T} = 1/(n_{A_T} \sigma_{\text{sp}, A_T})$  where the spallation cross section in milli-barns is given by  $\sigma_{\text{sp}, A_T} = 45 A_{A_T}^{0.7}$  mb (see Ouyed et al. 2011). The average number of collisions (i.e. the number of spallation mfps) an incoming neutron experiences in the target layer  $A_T$  is then

$$N_{\text{mfp}, A_T} \approx \frac{\Delta R_{A_T}}{\lambda_{\text{sp}, A_T}} \approx 0.69 \frac{M_{A_T, \text{SN}}/0.1 M_{\odot}}{(A_{T, 56})^{0.3} (v_{\text{sn}, 5000} t_{\text{delay}, 10})^2}, \quad (1)$$

where  $A_{T, 56}$  is the target atomic mass in units of 56 and  $0.1 M_{\odot}$  representative of the mass in the  $^{56}\text{Ni}$  layer. In the equation above,  $v_{\text{sn}}$  is given in units of  $5000 \text{ km s}^{-1}$  and is kept constant in all of the simulations shown in this paper. The time delay,  $t_{\text{delay}}$ , is in units of 10 days. For our fiducial values in mass of the target material and for  $t_{\text{delay}} = 10$  days we get  $N_{\text{mfp}, \text{Ni}} \sim 0.69$ ,  $N_{\text{mfp}, \text{S}} \sim 0.41$ ,  $N_{\text{mfp}, \text{Si}} \sim 0.42$ ,  $N_{\text{mfp}, \text{Mg}} \sim 0.44$ ,  $N_{\text{mfp}, \text{Ne}} \sim 0.47$ ,  $N_{\text{mfp}, \text{O}} \sim 15.10$ ,  $N_{\text{mfp}, \text{C}} \sim 1.64$  for spallation on  $^{56}\text{Ni}$ ,  $^{32}\text{S}$ ,  $^{28}\text{Si}$ ,  $^{24}\text{Mg}$ ,  $^{20}\text{Ne}$ ,  $^{16}\text{O}$ ,  $^{12}\text{C}$ , respectively.

In a regime where  $\lambda_{\text{sp}, A_T} > \Delta R_{A_T}$  (i.e.  $N_{\text{mfp}, A_T} < 1$ ), there will be minimal or even no spallation induced by the QN neutrons on the target  $A_T$  in which case most of the neutrons proceed onto the next, overlaying, layer. Thus, for a given  $M_{A_T, \text{SN}}$  and  $v_{\text{sn}}$  this defines a critical time delay above which no spallation occurs in layer of element  $A_T$ . This allows us to define four regimes in our model:

(i)  $t_{\text{delay}} > t_{\text{outer}}$  with minimal or no spallation occurring in the inner layers. It means that for  $t_{\text{delay}} > t_{\text{outer}} \approx 8.3 \text{ days} \times (M_{\text{Ni}, \text{SN}}/0.1 M_{\odot})^{1/2} / (A_{T, 56}^{0.15} v_{\text{sn}, 5000})$  days (see eq. 2 in Ouyed 2013), the QN neutrons barely interact with the inner layers and proceed directly to the outer (O and C layers);

(ii)  $t_{\text{delay}} < t_{\text{inner}}$  with spallation occurring mainly in the inner layers, beneath the oxygen layer, with  $t_{\text{inner}} \approx 6.3 \text{ days} \times (M_{\text{Ni}, \text{SN}}/0.1 M_{\odot})^{1/2} / (A_{T, 56}^{0.15} v_{\text{sn}, 5000})$  (see Eq. 6 in Ouyed 2013)<sup>4</sup>. This regime corresponds to the situation where the spallated (i.e. subsequent generations of) neutrons exiting the inner layers, do not have enough energy to spallate the outer CO-rich layers;

(iii)  $t_{\text{inner}} < t_{\text{delay}} < t_{\text{outer}}$  with spallation occurring both in the inner and outer layers. In this regime, the neutrons spallated in the inner layers end up with energies above the critical values for spallation in the  $^{16}\text{O}$  (and in certain cases in the  $^{12}\text{C}$ ) to ensue;

(iv)  $t_{\text{delay}} > t_{\text{no-spall}}$  which effectively defines a regime of a QN occurring in isolation since no interaction occurs between the SN and QN ejecta. For our

<sup>4</sup>In Ouyed (2013),  $t_{\text{outer}}$  and  $t_{\text{inner}}$  were defined as  $t_{\text{Ni}}$  and  $t_{\text{O}}$ , respectively.

fiducial values,  $t_{\text{no-spall}} \sim 23\text{-}24$  days. For  $t_{\text{outer}} < t_{\text{delay}} < t_{\text{no-spall}}$ , spallation would occur mainly in the oxygen and carbon layers.

- **The energy per nucleon,  $E_{\text{QN}}$ , in the neutron-rich QN ejecta:** It defines and sets the total multiplicity,  $\zeta$ , of the spallated (i.e. subsequent generations of) neutrons and protons and their energies. The average neutrons+proton multiplicity  $\zeta_{\text{av}}$  on target  $A_{\text{T}}$  is given in eq. (2) in Ouyed (2013) as

$$\zeta_{\text{av}} \simeq 7A_{\text{T},56} \times (1 + 0.38 \ln E_{\text{n}}), \quad (2)$$

where  $E_{\text{n}}$  is the neutron energy in GeV which leads to a subsequent generation of spallated neutrons and protons with energy  $\sim E_{\text{n}}/\zeta_{\text{av}}$ . The resulting spallation product's atomic weight will peak at  $A_{\text{T}} - \zeta_{\text{av}}$ . The  $\zeta_{\text{av}} > 1$  condition gives the minimum neutron energy necessary for spallation to occur in the Ni, S, Si, Mg, Ne, O, C layer to be  $E_{\text{sp},A_{\text{T}}} \sim 0.105, 0.139, 0.153, 0.173, 0.206, 0.268, 0.416$  GeV, respectively.

Table 1 shows results from simulations involving the interaction of  $E_{\text{QN}} = 5$  GeV and  $E_{\text{QN}} = 10$  GeV neutrons with the PopIII-SNII ejecta when  $t_{\text{delay}} = t_{\text{outer}} \simeq 8.3$  days. For our fiducial values of the targets' initial masses this time delay implies  $N_{\text{mfp,Ni}} \sim N_{\text{mfp,S}} \sim N_{\text{mfp,Si}} \sim N_{\text{mfp,Mg}} \sim N_{\text{mfp,Ne}} \sim 1$  which means that on average a QN neutron will interact once per layer. An  $E_0 = E_{\text{QN}} = 10$  GeV QN (primary) neutron would lead to a multiplicity of  $\zeta_{\text{av}} \sim 13$  in the  $^{56}\text{Ni}$  layer. This means a spallated (secondary generation of) neutrons and protons exiting the layer with energy  $E_1 = E_0/\zeta_{\text{av}} \sim 0.77$  GeV. These secondary nucleons induce an average multiplicity  $\zeta_{\text{av}} \sim 3.6$  in the  $^{32}\text{S}$  layer which yields spallated (tertiary generation of) neutrons and protons exiting the layer with energy  $\sim 0.21$  GeV. As can be seen from Table 1, spallation ceases at the Si layer since within the first three layers the neutrons energy has cascaded down to  $\sim 0.15$  GeV, below the critical value for Mg-spallation. The main (i.e. peak) spallation products are shown as well as the net multiplicity  $\zeta_{\text{net}}$  which yields a total mass of spallated neutrons and protons which amounts to  $M_{\text{n+p}} = \zeta_{\text{net}} M_{\text{QN}} \sim 0.05\text{-}0.1 M_{\odot}$ . This table shows the pathway of a typical neutron with the expected average multiplicity given by eq. (2). However, because the  $\zeta$  distribution is not uniform, some neutrons induce above average multiplicity ( $\zeta > \zeta_{\text{av}}$ ) and stop within the  $^{56}\text{Ni}$  layer while those inducing below average multiplicity ( $\zeta < \zeta_{\text{av}}$ ) make it past the inner layers and induce spallation in the oxygen layer (see discussion below).

Another example is shown in Table 2 which shows results from the interaction of  $E_{\text{QN}} = 5$  GeV and  $E_{\text{QN}} = 10$  GeV neutrons with the PopIII-SNII ejecta when  $t_{\text{delay}} > t_{\text{outer}}$  (here  $t_{\text{delay}} = 12$  days). For our fiducial values,  $N_{\lambda_{\text{sp},\text{O}}} \sim 10$  and  $E_{\text{sp},\text{O}} \sim 0.27$  GeV. As can be seen from Table 2, neutrons interact with five sub-layers (each representing a spallation mfp) before their energy cascade down below 0.268 GeV. Thus half the amount of oxygen in the PopIII-SNII will be destroyed forming sub-O products. In each sub-layer denoted by index  $i$  (i.e. for each mfp, or  $\lambda_{\text{sp},\text{O}}$ ), the atomic weight of the spallation products is close to a normal distribution peaking at atomic weight  $A_{\text{peak},i} \sim A_{\text{T}} - \zeta_{\text{av},i}$ . The final

abundances of the spallation products is a combination of these distributions (see Figure 1 in Ouyed et al. 2011). As can be seen in Table 2 the total spallation neutrons and protons amounts to  $M_{n+p} = \zeta_{\text{net}} M_{\text{QN}} \sim 0.02\text{-}0.04 M_{\odot}$ . This Table further illustrates the important point that most of the spallated neutrons exiting the oxygen layer will not be able to induce spallation in the overlaying C layer since their energy is below the threshold for C-spallation ( $\sim 0.42$  GeV). See however discussion below.

We end this subsection by mentioning some important points:

(i) The true  $\zeta$  distribution is not uniform and is rather close to a normal distribution peaking at  $\zeta_{\text{av.}}$ . This means that the spallated neutrons would exit a sub-layer  $i$  of the target material ( $A_{\text{T}}$ ) with a non-uniform energy distribution peaking at  $\sim E_i/\zeta_{\text{av.,i}}$ . For the case shown in Table 2, most of the neutrons spallated in the oxygen layer will not be able to induce spallation in the overlaying C layer – since their energy is below the threshold for C-spallation  $E_{\text{sp.,C}} \sim 0.42$  GeV. However, neutrons leading to a multiplicity  $\zeta < \zeta_{\text{av.}}$  do induce spallation after exiting the oxygen layer. As we show later (see §4.1.1), this has important consequences to production of  ${}^7\text{Li}$  from spallation in the C-layer;

(ii) The logarithmic energy dependence of  $\zeta_{\text{av.}}$  means that there is little difference between the multiplicity distribution induced by the  $E_{\text{QN}} = 10$  GeV and the  $E_{\text{QN}} = 5$  GeV neutrons. However, for the lower energy primaries with  $E_0 = E_{\text{QN}}$  (i.e. QN neutrons), the resulting average energy per spallated nucleon is lower. In the case of spallation in the Oxygen layer for example (as illustrated in Table 2), the  $E_{\text{QN}} = 5$  GeV simulations shows fewer neutrons with energy above  $E_{\text{sp.,C}} \sim 0.42$  GeV making it past the oxygen layer; i.e. spallation in the overlaying C-layer is reduced as compared to the  $E_{\text{QN}} = 10$  GeV simulations (discussed further in §4.1.1);

(iii) Even if the spallation condition,  $E_n > E_{\text{sp.,AT}}$ , is satisfied in any layer of target material  $A_{\text{T}}$  (a necessary condition), it is not sufficient when  $\lambda_{\text{sp.,AT}} > \Delta R_{\text{AT}}$ ; i.e. when the spallation mfp exceeds the thickness of the target layer (see discussion following eq. 1). Thus the  $E_n > E_{\text{sp.,AT}}$  and the  $\Delta R_{\text{AT}} > \lambda_{\text{sp.,AT}}$  must be satisfied simultaneously.

### 3.2. ${}^{56}\text{Ni}$ destruction and Iron-impooverishment in our model

#### 3.2.1. The $t_{\text{delay}}$ -[Fe/H] connection

Following spallation in the  ${}^{56}\text{Ni}$  layer, the resulting iron abundance ([Fe/H]) in the primordial cloud swept by the combined SN+QN ejecta is (eq. 5 in Ouyed 2013):

$$\left[ \frac{\text{Fe}}{\text{H}} \right] = \log \eta_{56}^{56} + \log \frac{M_{\text{Ni,SN}}/0.1M_{\odot}}{M_{\text{sw}}/10^5M_{\odot}} - 3.12, \quad (3)$$

where  $\eta_{\text{A}}^{\text{AT}} = M_{\text{A}}/M_{\text{AT,SN}}$  is the normalized mass yields of product/element A following spallation on target  $A_{\text{T}}$  (originally present in the SN ejecta; here 56 refers to



$^{56}\text{Ni}$ ). Here  $M_{\text{sw}}$  is the mass swept up by the mixed SN+QN ejecta in the primordial pristine cloud surrounding the site of the dsQN explosion;  $M_{\text{sw}}$  is in units of  $10^5 M_{\odot}$  (e.g. Shigeeyama&Tsujimoto 1998; Machida et al. 2005).

In our model, a dsQN with a given  $t_{\text{delay}}$  translates to a corresponding  $[\text{Fe}/\text{H}]$  abundance in the swept up cloud; this is set by the parameter  $\eta_{56}^{56}$  which is the level of depletion of the original PopIII-SNII  $^{56}\text{Ni}$  following spallation. Figure 1 in Ouyed (2013) shows the heavy depletion of the original PopIII-SNII  $^{56}\text{Ni}$  by spallation obtained for very short time delays ( $t_{\text{delay}} < 2$  days) where  $\eta_{56}^{56} < 10^{-4}$  (i.e. leading to  $[\text{Fe}/\text{H}] < -7$ ). Hyper metal-poor stars (HMPs with  $[\text{Fe}/\text{H}] < -5$  in the terminology of Beers&Christlieb 2005) would form from clouds swept up by  $t_{\text{delay}} < 3$  days dsQNe in our model (see §5).

In dsQNe with long enough delays (i.e.  $t_{\text{delay}} > t_{\text{outer}}$ ), there is minimal spallation in the  $^{56}\text{Ni}$  layer (i.e.  $\eta_{56}^{56} \simeq 1$ ) and in the innermost layers ( $^{32}\text{S}$ ,  $^{28}\text{S}$ ,  $^{24}\text{Mg}$ ) layers. For such dsQNe, high values of  $[\text{Fe}/\text{H}]$  are obtained by increasing  $M_{\text{Ni,SN}}$  or by decreasing the amount of swept up material,  $M_{\text{sw}}$  (see eq. 3 above). For example, a dsQN with  $t_{\text{delay}} > 10$  days,  $M_{\text{Ni,SN}} = 0.5 M_{\odot}$  and  $M_{\text{sw}} = 10^{4.5} M_{\odot}$  gives  $[\text{Fe}/\text{H}] \sim -1.9$ .

### 3.2.2. Sub-Fe elements

Shown in Figure 1 in this paper are abundances of sub-Fe spallation products resulting from dsQNe with different  $t_{\text{delay}}$ ; shown is the relative abundance  $[X/\text{Fe}]$ . The original composition of the PopIII-SNII ejecta is shown by the plus signs in all of the panels. These elements are identified by an asterisk next to their names in all of the panels as their abundances vary with  $t_{\text{delay}}$ .

For  $t_{\text{delay}} > t_{\text{no-spall}} \sim 23\text{-}24$  days (not shown here) no spallation occurs and the original elements (identified with an asterisk) fall exactly on the plus signs. For  $t_{\text{outer}} \sim 8.3$  days  $< t_{\text{delay}} < t_{\text{no-spall}}$ , there is minimal interaction in the inner layers and most spallation products are light elements from O- and C-spallation. The original relative abundance of the PopIII-SNII elements is almost conserved except for some spallation in the oxygen layer which leads to the formation of B, Be and Li. For intermediate  $t_{\text{delay}}$  (i.e.  $t_{\text{inner}} \sim 6.3$  days  $< t_{\text{delay}} < t_{\text{outer}}$ ), spallation occurs in almost all of the layers. As  $t_{\text{delay}}$  gets shorter spallation efficiency starts to decrease in the outer layers and eventually for  $t_{\text{delay}} < \sim 6$  days spallation starts to become more prominent in the innermost layers. For even shorter  $t_{\text{delay}}$  (top panels), most of the QN neutrons are used up in the  $^{56}\text{Ni}$  layer thus shielding all of the overlying layers. Effectively, the original PopIII-SNII sub-Ni elements (S, Si, Mg, Ne, O, C) present in the PopIII-SNII ejecta would be preserved in dsQNe with very short delays. In addition these elements will be produced as by-products of spallation in the  $^{56}\text{Ni}$  layer which further increases their overall  $[X/\text{Fe}]$  values for  $t_{\text{delay}} < 3$  days. The weak-dependency of multiplicity on the neutrons' energy explains the nearly similar final abundances for the  $E_{\text{QN}} = 5$  GeV and the  $E_{\text{QN}} = 10$  GeV simulations.

### 3.2.3. $\alpha$ -elements

The so-called  $\alpha$ -elements (O, Ne, Mg, Si, S, Ca, Ti) in very metal-poor stars are reported to be overabundant relative to iron at low metallicity (e.g. McWilliam 1997;

Aoki et al. 2007) with  $[\alpha/Fe] > [\alpha/Fe]_{\odot}$  where  $[\alpha/Fe] = \frac{1}{4}([\text{Mg}/\text{Fe}] + [\text{Si}/\text{Fe}] + [\text{Ca}/\text{Fe}] + [\text{Ti}/\text{Fe}])$  (the average abundance of Mg, Si, Ca and Ti). These enhancements increase linearly with decreasing metallicity.

Figure 2 shows the relative abundances of the original PopIII-SNII elements with respect to  $t_{\text{delay}}$  (top panel) and metallicity (lower panel) for simulations with  $E_{\text{QN}} = 5$  GeV. Figure 3 shows the results for the  $E_{\text{QN}} = 10$  GeV simulations. For  $t_{\text{delay}} > t_{\text{outer}} \sim 8.3$  days,  $[X/Fe]$  remain close to the original values except for oxygen which experiences some spallation and thus depletion up to  $t_{\text{delay}} \sim 15$  days since it is by far the most abundant PopIII-SNII element. For  $t_{\text{inner}} < t_{\text{delay}} < t_{\text{outer}}$ , spallation occurs in most of the PopIII-SNII layers leading to an overall reduction in the abundances of the original elements. This leads to a dip in the  $[X/Fe]$  values in Figure 2 and in Figure 3 for  $-4 < [\text{Fe}/\text{H}] < -3$ . A plateau-like behaviour is noticeable in the dip for all of the PopIII-SNII elements. The  $[\text{Si}/\text{Fe}]$  and  $[\text{Mg}/\text{Fe}]$  levels in the dip region, combined with the copious production of Ti and Ca from Ni-spallation (see Figure 1) lead to  $[\alpha/Fe] > [\alpha/Fe]_{\odot}$  in our model and in particular for  $t_{\text{delay}} < t_{\text{outer}} \sim 8.3$  days (i.e.  $[\text{Fe}/\text{H}] < -3$ ) since spallation is more pronounced in the  $^{56}\text{Ni}$  layer than in the overlaying layers.

An increase of  $[X/Fe]$  is evident for most elements when the metallicity decreases below  $\sim -4$ ; i.e. when  $t_{\text{delay}}$  decreases below roughly 5 to 6 days. These layers are shielded at the expense of  $^{56}\text{Ni}$  depletion explaining the increase in  $[X/Fe]$  much above the initial values. In general, and for short  $t_{\text{delay}}$  in our model, the more abundant a specific element is in the PopIII-SNII shocked ejecta, prior to spallation by the QN neutrons, the more it will appear abundant following the destruction of  $^{56}\text{Ni}$  (i.e. the reduction of the final iron abundance in the swept up cloud). Since O and C are the two-most abundant elements in the PopIII-SNII ejecta, it is no surprise that  $[\text{C}/\text{Fe}]$  and  $[\text{O}/\text{Fe}]$  are very enhanced for very short delays (see below for the special case of  $^{32}\text{S}$ ). These enhancement would be reflected in the composition of the gas cloud swept up by the SN+QN ejecta out of which the Pop. II low-mass stars would form.

#### 3.2.4. Sulfur

Figures 2 and 3 show that Sulfur is more depleted (with  $[\text{S}/\text{Fe}]$  showing the lowest plateau in the dip) than the other original elements in the PopIII-SNII ejecta for  $6.3 \text{ days} < t_{\text{delay}} < 8.3 \text{ days}$  (i.e.  $-4 < [\text{Fe}/\text{H}] < -3$ ) due to its close proximity to the Nickel layer. Even for very short delays, because of the non-uniform distribution in multiplicity  $\zeta$ , some spallated neutrons in the  $^{56}\text{Ni}$  manage to make it to the overlaying  $^{32}\text{S}$  layer. This explains why the  $^{32}\text{S}$  plateau in the dip extends to metallicity as low as  $[\text{Fe}/\text{H}] \sim -4$ . Only for  $t_{\text{delay}} < 5$  days (i.e.  $[\text{Fe}/\text{H}] < -4$ ) does it become completely shielded and starts to follow the behavior of the other elements by increasing with decreasing  $[\text{Fe}/\text{H}]$ .  $^{32}\text{S}$  has another distinctive feature:  $[\text{S}/\text{Fe}]$  exceeds  $[\text{C}/\text{Fe}]$  at very low metallicity despite the higher initial abundance of C as compared to S in the PopIII-SNII ejecta. It turns out that Sulfur is among the main spallation products from Ni-spallation for  $t_{\text{delay}} < 5$  days (i.e.  $[\text{Fe}/\text{H}] \sim -4$ ). This produced S adds to the original S which explains why  $[\text{S}/\text{Fe}]$  exceeds  $[\text{C}/\text{Fe}]$  for our fiducial values. The trend of  $[\text{S}/\text{Fe}]$  versus  $[\text{Fe}/\text{H}]$  in extremely metal-poor stars awaits monitoring and

observations before its dependence on metallicity are known with higher accuracy (e.g. Nissen et al. 2007; Spite et al. 2011 and references therein). Only then can our model be put to test.

### 3.2.5. Comparing to the average star

Figure 4 is a comparison of yields from a typical dsQN experiencing spallation in the inner and outer layers (i.e. in the  $t_{\text{inner}} < t_{\text{delay}} < t_{\text{outer}}$  regime which corresponds to  $-4 < [\text{Fe}/\text{H}] < -3$  in our model); we chose  $t_{\text{delay}} = 6.5$  days. Our simulation results are compared to abundance pattern shared by stars in the metallicity range  $-4.0 < [\text{Fe}/\text{H}] < -3.0$  with a normal  $[\text{C}/\text{Fe}]$  ratio (Cayrel et al. 2004; Spite et al. 2005; see also Figure 1 in Limongi&Chieffi 2012). As can be seen from Figure 4, both the  $E_{\text{QN}} = 10$  GeV and  $E_{\text{QN}} = 5$  GeV simulations are successful in reproducing the observed abundances. Note the the high abundances of Fluorine and Scandium which are spallated in the innermost layers in our model; these two rare elements are natural products of spallation (see §6.2 in Ouyed (2013)). The  $E_{\text{QN}} = 5$  GeV simulations underestimate the  $[\text{C}/\text{Fe}]$  and  $[\text{O}/\text{Fe}]$  abundances but this is easily remedied by increasing the original carbon and oxygen content in the PopIII-SNII ejecta to reasonable amounts.

### 3.3. Nitrogen in our model

As shown in Ouyed (2013; see §3.3 in that paper),  $^{14}\text{N}$  forms by spallation in the  $A > 14$  layers in the PopIII-SNII ejecta. However, we find that  $^{14}\text{N}$  can also be enhanced by the injection of protons from spallation into the C-rich and O-rich outer layers if temperatures in the PopIII-SN ejecta exceeds  $\sim 1.6 \times 10^7$  K when it is hit by the QN ejecta. The carbon (and perhaps oxygen) could subsequently be processed into  $^{14}\text{N}$  via the CN(O) cycle (Arnett 1996). For an adiabatic expansion of the preceding SN shell (i.e.  $T_{\text{env.}} \propto t^{-2}$ ), the  $T_{\text{env.}} > 1.6 \times 10^7$  K necessary condition for CN (proton capture) process to take place yields

$$t_{\text{delay}} < \sim 5 \text{ days} \frac{R_{\text{prog.,100}} T_{\text{env.,10}}^{1/2}}{v_{\text{sn,5000}}}, \quad (4)$$

where  $R_{\text{prog.,100}}$  is the initial radius of the progenitor in units of  $100R_{\odot}$  ( $R_{\odot}$  is the solar radius) and  $T_{\text{env.,10}}$  the initial temperature of the PopIII-SNII envelope in units of  $10^{10}$  K. For our fiducial parameters, the above translates to (see Figure 1 in Ouyed 2013)

$$\left[ \frac{\text{Fe}}{\text{H}} \right] < -4. \quad (5)$$

We find that the CN(O) processing of a small percentage ( $< 10\%$ ) of the carbon and oxygen into  $^{14}\text{N}$  is enough to account for the observed  $[\text{N}/\text{Fe}]$  values in an average star (in Figure 4 the CN enhanced nitrogen is identified with a filled diamond). The  $^{13}\text{C}$  abundance should also be enhanced if CN equilibrium is established in which case the  $^{12}\text{C}/^{13}\text{C}$  ratios should be of the order of a few (see however Caughlan & Fowler 1972). In our model,  $^{14}\text{N}$  production from CN cycling could occur at higher

[Fe/H] when taking into account envelope reheating by the QN shock (following impact on the SN ejecta). However, we caution that our model is more detailed than the standard CN cycle and would need further investigations for better estimates of  $^{14}\text{N}$  enhancement and the expected  $^{12}\text{C}/^{13}\text{C}$  values.

#### 4. LITHIUM SYNTHESIS IN OUR MODEL

The  $^7\text{Li}$  produced by spallation on a target  $A_T$  in the ejecta of the PopIII-SNII ejecta is given by eq.(14) in Ouyed (2013):

$$A(\text{Li}) \simeq \log \eta_7^{A_T} + \log \frac{M_{A_T, \text{SN}}/1.5M_\odot}{M_{\text{sw}}/10^5 M_\odot} + 6.33, \quad (6)$$

where  $\eta_7^{A_T} = M_{7\text{Li}}/M_{A_T, \text{SN}}$  is the normalized mass yields of  $^7\text{Li}$  following spallation on target  $A_T$  with initial mass  $M_{A_T, \text{SN}}$ ; the  $1.5M_\odot$  is representative of our fiducial value for the oxygen content in mass in the PopIII-SNII ejecta. The final  $^7\text{Li}$  abundance is a combination of  $^7\text{Li}$  produced from spallation on each of the targets present in the PopIII-SNII ejecta.

Shown in Figure 5 is the  $^7\text{Li}$  abundances resulting from spallation by  $E_{\text{QN}} = 5$  GeV (left panels) and  $E_{\text{QN}} = 10$  GeV (right panels) QN neutrons on a typical PopIII-SNII ejecta in our model. The top panels show  $A(\text{Li})$  from simulations spanning a range in  $^{56}\text{Ni}$  content of the PopIII-SII ejecta ( $0.05M_\odot \leq M_{\text{Ni}, \text{SN}} \leq 0.5M_\odot$ ) and a range in  $t_{\text{delay}}$  (2 days  $\leq t_{\text{delay}} \leq 24$  days). The bottom panels show the corresponding metallicity [Fe/H]; as explained in 3.2.1 there is a direct connection between  $t_{\text{delay}}$  and [Fe/H] in our model. For  $t_{\text{delay}} > 24$  days the QN neutrons traverse the PopIII-SNII ejecta with minimal interaction; i.e. no spallation occurs and the PopIII-SNII ejecta abundances would not be modified or affected (i.e.  $\eta_A^{A_T} = 1$ ). While  $^{56}\text{Ni}$  content was varied, the other initial abundances in mass in the PopIII-SNII were set to their fiducial values:  $M_{\text{S}, \text{SN}} = M_{\text{Si}, \text{SN}} = M_{\text{Mg}, \text{SN}} = M_{\text{Ne}, \text{SN}} = 0.05M_\odot$ ,  $M_{\text{O}, \text{SN}} = 1.5M_\odot$  and  $M_{\text{C}, \text{SN}} = 0.15M_\odot$ . We adopt a  $10^5 M_\odot$  of pristine cloud (the cradle of the Pop. II low-mass stars) swept up by the SN+QN ejecta (e.g. Shigeyama&Tsujimoto 1998).

The different panels in Figure 6 (Figure 8) show the resulting  $A(\text{Li})$  versus  $t_{\text{delay}}$  for each target for the  $E_{\text{QN}} = 5$  GeV ( $E_{\text{QN}} = 10$  GeV) simulations. The corresponding  $A(\text{Li})$  versus [Fe/H] is shown in Figure 7 (Figure 9). The lower right panel in Figure 6 (Figure 8) shows the combined  $A(\text{Li})$  versus  $t_{\text{delay}}$  which effectively corresponds to the projection of the upper left (right) panel in Figure 5 onto the  $A(\text{Li})$ - $t_{\text{delay}}$  plane. Similarly, the lower right panel in Figure 7 (Figure 9) shows the combined  $A(\text{Li})$  versus [Fe/H] which effectively corresponds to the projection of the lower left (right) panel in Figure 5 onto the  $A(\text{Li})$ -[Fe/H] plane. One can see from these panels that  $^7\text{Li}$  is produced in the  $^{56}\text{Ni}$  and  $^{32}\text{S}$  layers when  $t_{\text{delay}} < t_{\text{outer}}$  and in the oxygen and carbon layers for longer delays ( $t_{\text{outer}} \sim 8.3$  days is shown by the vertical dashed lines in the figures). No  $^7\text{Li}$  is spallated in the intermediate layers (Si, Mg, Ne) and in general  $^7\text{Li}$  is mainly produced either in the innermost layers or in the outermost CO layers. The vertical dotted lines defines the  $N_{\text{mfp}, \text{C}} = \Delta R_{\text{C}}/\lambda_{\text{sp}, \text{C}} = 1$  boundary which defines a timescale above which the spallation mfp exceeds the thickness of the C-layer; i.e. no C-spallation occurs for longer time delays even if the neutrons

exiting the O-layer have energies exceeding  $E_{\text{sp},\text{C}} \sim 0.42$  GeV which is above the critical value for C-spallation to ensue.

There is a gap in the  ${}^7\text{Li}$  abundance (i.e. a drop in the  $A(\text{Li})$  value) in the intermediate regime,  $t_{\text{inner}} < t_{\text{delay}} < t_{\text{Ni}}$  (which corresponds to  $-4 < [\text{Fe}/\text{H}] < -3$ ) since most neutrons end up being used for spallation of  $A > 7$  elements in the inner layers. Thus, for Pop. II low-mass stars formed from clouds swept up by dsQNe with  $t_{\text{delay}} < 8.3$  days (i.e. for  $[\text{Fe}/\text{H}] < -3$ ), the resulting  ${}^7\text{Li}$  abundance would show a larger scatter mainly because in these dsQNe  ${}^7\text{Li}$  is not the main spallation product and the neutrons are used up to make many other spallation products. At this point, we must note that the  ${}^7\text{Li}$  abundance in dsQNe leading to  $[\text{Fe}/\text{H}] < -3$  (i.e. in  $t_{\text{delay}} < \sim 10$  days dsQNe) should be considered upper limits in our model. For such dsQNe, the SN ejecta is still hot ( $T > 2.5 \times 10^6$  K) when it is spallated. Combined with the copious production of protons (see Tables 1 and 2), we expect most of the spallated  ${}^7\text{Li}$  to be destroyed by reactions with the protons or at least become reduced (see §5 in Ouyed 2013).

#### 4.1. The high-scatter; $A(\text{Li}) \sim 2.2$ , plateau

Two ‘‘plateaus’’ can be seen in the top right panel in Figure 5 (i.e. for the  $E_{\text{QN}} = 10$  GeV simulation). One resulting from O-spallation with  $1.8 < A(\text{Li}) < 2.5$  and a second one from C-spallation with  $2.5 < A(\text{Li}) < 3.5$ . These two plateaus can also be seen in panels labeled ‘‘C-Target’’ and ‘‘O-Target’’ in Figures 6, 7, 8, 9. Both occur for  $t_{\text{delay}} > t_{\text{outer}} \sim 8.3$  days which means that the QN neutrons proceed directly into the outer layers with minimal interaction with the Ni, S, Si, Mg and Ne layers. Spallation in the O-layer leads to smaller  ${}^7\text{Li}$  abundance and more scatter in the  ${}^7\text{Li}$  plateau since the neutrons spallate more products than in the case of spallation in the C-layer.

We first focus on the  $A(\text{Li}) \sim 2.2$  plateau uncovered in our simulations (the  $A(\text{Li}) = 2.2$  value is indicated by the horizontal planes in Figure 5 and by the horizontal lines in Figures 6, 7, 8, 9). This plateau is populated by  ${}^7\text{Li}$  spallated from oxygen for dsQNe with  $t_{\text{delay}} > 8.3$  days. As can be seen from Figure 5, while the  $E_{\text{QN}} = 5$  GeV simulations yield  $A(\text{Li})$  approaching the 2.2 value from the lower bound, barely exceeding it, the  $E_{\text{QN}} = 10$  GeV simulations yield  ${}^7\text{Li}$  abundances oscillating around  $A(\text{Li}) \sim 2.2$  (with  $1.8 < A(\text{Li}) < 2.5$ ). To understand this interesting finding from our simulations we first note that in each sub-layer  $i$  (i.e. for each mfp,  $\lambda_{\text{sp},\text{O}}$ ) of the O-layer, the distribution of the atomic weights of the spallation products is close to a normal distribution peaking at  $A_{\text{peak},i} \sim A_{\text{T}} - \zeta_{\text{av},i}$  where  $\zeta_{\text{av},i}$  is the average multiplicity for sub-layer  $i$  (see Table 2). For each sub-layer the corresponding amount in mass of spallated  ${}^7\text{Li}$  can be estimated from the corresponding distribution.

Since the highest  $\zeta_{\text{av}}$  is induced in the first sub-layer this leads to a peak spallation product ( $A_{\text{peak}} = 16 - \zeta_{\text{av}}$ ) closest to  ${}^7\text{Li}$ . Subsequent sub-layers would yield peak spallation products getting closer to the target’s  $A_{\text{T}}$  (here  $A_{\text{T}} = 16$ ) thus reducing the  ${}^7\text{Li}$  contribution to the overall distribution of the spallated elements and thus a reduction in the final amount of  ${}^7\text{Li}$  spallated. However, for subsequent sub-layers the multiplicity is higher and more neutrons+protons induce spallation. The final abundances of the spallation products is a combination of these distributions (see e.g. Figure 1 in Ouyed et al. 2011) which yields  $M_{\text{Li}} \sim \alpha_7 \zeta_{\text{net}} M_{\text{QN}} \equiv \beta_7 M_{\text{QN}}$  where

$\beta_7 = \alpha_7 \zeta_{\text{net}}$ . Since the  ${}^7\text{Li}$  contribution given by the distributions is roughly  $\alpha_7 \sim 0.01$  (of the order of  $\sim 1\%$ ) and  $\zeta_{\text{net}} \sim 10$  (see e.g. Table 2) this yields  $\beta_7 \sim 0.1$ . The corresponding  ${}^7\text{Li}$  abundance  $A(\text{Li}) = \log N_{7\text{Li}}/N_{\text{H}} + 12$  is then roughly estimated to be

$$A(\text{Li}) \sim 2.15 + \log\left(\beta_{7,0.1} \frac{M_{\text{QN}}/10^{-3}M_{\odot}}{M_{\text{sw}}/10^5M_{\odot}}\right), \quad (7)$$

where we made use of  $N_{7\text{Li}} = M_{7\text{Li}}/7m_{\text{H}}$  and  $N_{\text{H}} = M_{\text{sw}}/m_{\text{H}}$ . The amount of  ${}^7\text{Li}$  spallated is roughly equivalent to a normalized mass yield  $\eta_7^{16} \sim 6.7 \times 10^{-5}$  or  $\log \eta_7^{16} \sim -4.17$  for our fiducial values; i.e.  $A(\text{Li}) \sim 2.15$  from using eq.(6).

The weak dependence of the multiplicity on energy leads to similar distributions of spallation products in the oxygen layer for the range in  $E_{\text{QN}}$  expected in QNe explosions. This translates to similar  $\zeta_{\text{net}}$  and  $\alpha_7$  (i.e.  $\beta_7$ ) values which explains why the  $E_{\text{QN}} = 5$  GeV also hovers around the same  $A(\text{Li})$  value and effectively implies that  $A(\text{Li})$  is mainly dependent on  $M_{\text{QN}}$  and  $M_{\text{sw}}$ . In fact by scaling  $M_{\text{sw}}$  with  $M_{\text{QN}}$  (i.e. with the kinetic energy,  $E_{\text{QN}}^{\text{KE}}$ , of the QN ejecta) we always recover an  $A(\text{Li})$  close to Spite values when  $t_{\text{delay}} > t_{\text{outer}}$ ; i.e. when spallation occurs mainly in the outer oxygen and carbon layers as shown in §4.2 below.

#### 4.1.1. The C-spallated ${}^7\text{Li}$ plateau

When  $\Delta R_{\text{C}} < \lambda_{\text{sp},\text{C}}$ , even if enough neutrons with energy above  $E_{\text{sp},\text{C}} \sim 0.42$  GeV make it past the O-layer, they will not interact with the overlaying carbon and there will be no spallated  ${}^7\text{Li}$  and the corresponding plateau would disappear. From eq. (1), the  $N_{\text{mfp},\text{C}} > 1$  condition (i.e.  $\Delta R_{\text{C}} > \lambda_{\text{sp},\text{C}}$ ) yields  $t_{\text{delay}} < \sim 13$  days  $\times (M_{\text{C},\text{SN}}/0.15M_{\odot})^{1/2}$  for our fiducial values. This means that spallation in the C-layer would occur mainly when  $t_{\text{outer}} \sim 8$  days  $< t_{\text{delay}} < 13$  days which is a narrow window. On the other hand, if we increase the carbon content in the PopIII-SNII ejecta as to make  $\Delta R_{\text{C}} > \lambda_{\text{sp},\text{C}}$  then spallation would ensue. Figure 10 shows the two plateaus again for  $E_{\text{QN}} = 10$  GeV but for much higher carbon content than our fiducial values (here  $M_{\text{C},\text{SN}} = M_{\text{O},\text{SN}} = 1.5M_{\odot}$ ). As can be seen in the figure, although the plateau from O-spallation is close to the Spite value, it is clearly dwarfed by the  ${}^7\text{Li}$  produced in carbon layer. For  $M_{\text{C},\text{SN}} = 1.5M_{\odot}$ , the  $\Delta R_{\text{C}} < \lambda_{\text{sp},\text{C}}$  regime occurs when  $t_{\text{delay}} > 30$  days beyond which the C-spallated  ${}^7\text{Li}$  plateau disappears. We find that in PopIII-SNII with high carbon content, and in particular those with  $E_{\text{QN}} \geq 10$  GeV, the  ${}^7\text{Li}$  plateau from C-spallation is dominant and far exceeds the Spite value. Another possibility would consist of reducing oxygen content in the PopIII-SNII ejecta so that the primary (i.e. QN) neutrons experience only a very few interactions (mfps) in the oxygen layer before making their way towards the C-layer. This is the least likely scenario since it seems that oxygen is produced in much larger quantity than carbon in PopIII-SNII ejecta (e.g. Umeda&Nomoto 2002).

On average, spallated neutrons in the  $E_{\text{QN}} = 5$  GeV case acquire lower energies than the  $E_{\text{QN}} = 10$  GeV case. Thus, there is no substantial amounts of  ${}^7\text{Li}$  spallated in the C-layer since fewer  $> 0.42$  GeV neutrons manage to make past the O-layer. The resulting plateau is very scattered and remains below Spite values; see the panels labeled ‘‘C-Target’’ in Figures 6 and 7.

#### 4.2. A low-scatter, $A(\text{Li}) \sim 2.2$ , plateau

If we associate high  $E_{\text{QN}}$  dsQNe with short time delays and low  $E_{\text{QN}}$  dsQNe with relatively longer delays ( $> 15$  days), a low-scatter plateau results as shown in Figure 11. The top panel shows abundances from simulations with  $E_{\text{QN}} = 10$  GeV and  $M_{\text{sw}} = 10^5 M_{\odot}$  with 5 days  $< t_{\text{delay}} < 15$  days. The middle panel shows results from an  $E_{\text{QN}} = 5$  GeV simulation with  $M_{\text{sw}} = 10^{4.5} M_{\odot}$  and for 15 days  $< t_{\text{delay}} < 30$  days. The combined  ${}^7\text{Li}$  abundance from these simulations leads to a plateau with features reminiscent of the observed one. To extend the plateau to higher  $[\text{Fe}/\text{H}]$  values we had to include simulations where the mass of the pristine cloud swept up by the dsQN is lower than the fiducial value of  $10^5 M_{\odot}$ . For example, the  $M_{\text{sw}} = 10^{4.5} M_{\odot}$  simulations effectively shift the plateau to the right in Figures 7 and 9 by yielding  $[\text{Fe}/\text{H}]$  values close to  $\sim -2$  (see eq. 3). However, a decrease in  $M_{\text{sw}}$  increases the  $A(\text{Li})$  value (see eq. 6) which is remedied by a decrease in  $E_{\text{QN}}$  which decreased the amounts of spallated  ${}^7\text{Li}$  accordingly. The high  $A(\text{Li}) \sim 3.5$  values in the top panel correspond to abundances from C-spallation. However, the thinnest plateaus result from simulations which minimize spallation in the C-layer. This meant setting  $M_{\text{C,SN}} < 0.1 M_{\odot}$  for our fiducial values, or in general by taking  $M_{\text{C,SN}} < M_{\text{O,SN}}/10$ .

While more sophisticated calculations may be required to further constrain the parameters, the QN model naturally explains this dichotomy: In general, the reduced mass-loss in Pop. III stars means that the more massive progenitors could in principle end up with the more massive cores at explosion and should thus lead to heavier NSs. Or, if fallback is greater from the more massive QN progenitors (i.e. those closer to the black hole limit which we set here to be  $40 M_{\odot}$ ), this should also translate to the formation of a more massive compact remnant (i.e. a parent NS with higher core density). These heavier NSs should undergo a QN explosion on shorter time delays as found by Staff et al. (2006). The core-collapse of the massive progenitors followed by the QN explosion of the massive NS would likely lead to a more energetic SN+QN ejecta which should sweep up more pristine material (i.e.  $M_{\text{sw}}$  should be higher in these dsQNe; e.g. Shigeyama&Tsujimoto 1998). Naturally, the shorter time delay (i.e. the lower  $[\text{Fe}/\text{H}]$ ) dsQNe would lead to a higher scatter in the plateau, and its eventual meltdown for the shortest delay dsQNe, since  ${}^7\text{Li}$  will be produced in the inner layers from multiple targets. In this picture, low-mass Pop. II stars in the Spite plateau would have originated from pristine clouds swept up by dsQNe with progenitors in the lower end of the mass range,  $20 M_{\odot} < M_{\text{prog.}} < 40 M_{\odot}$ , with reduced fallback. As discussed later (see §5), dsQNe with short delays should be the rarest among dsQNe. The implication is that the resulting Pop. II stars (those with very low  $[\text{Fe}/\text{H}]$  and high  $A(\text{Li})$  scatter according to our model) would be the rarest among very metal-poor stars.

#### 4.3. Discussion

We now discuss some implications of our findings to Lithium in the Universe:

- **The BBN component:** In this work and in Ouyed (2013), we have neglected the BBN contribution in the cloud swept up by the SN+QN ejecta and considered only  $A(\text{Li})$  from dsQN spallation on PopIII-SNII ejecta. Among plausible

scenarii that could lead to the destruction of the BBN component in pristine clouds, before they get swept up by the combined SN+QN ejecta, are:

(i) The QN provides copious amount of neutrons with some of them freely streaming ahead of the combined SN+QN ejecta. These free QN neutrons could destroy the BBN  ${}^7\text{Li}$  (e.g., see Albornoz Vásquez et al. 2012 and references therein for relevant nuclear reactions). This might contribute to the destruction of the surrounding BBN  ${}^7\text{Li}$  before material is swept up by the SN+QN ejecta – this remains to be confirmed;

(ii) A massive astration of  ${}^7\text{Li}$  by processing in Pop. III stars as suggested by Piau et al. (2006). This model provides a natural connection to ours since it appeals to Pop. III stars in the  $10M_{\odot}$ - $40M_{\odot}$  mass range; the favored QN progenitor mass range. Thus, adopting the Piau et al. (2006) hypothesis, one could then envision a scenario in which the BBN  ${}^7\text{Li}$  is processed and destroyed by the Pop. III star before it undergoes a PopIII-SNII explosion and the subsequent QN event. In this scenario, the issue of overproduction of CNO elements plaguing the Piau et al. (2006) hypothesis is alleviated since in our scenario these would be reduced by spallation. The pristine material/cloud swept up would then carry the imprint of  ${}^7\text{Li}$  resulting from spallation of PopIII-SNII ejecta by dsQNe without the overproduction of CNO elements;

(iii) The last and the most bold proposition is the one where we envisage that  ${}^7\text{Li}$  might not have been processed during BBN and is rather a relic of primordial dsQNe spallation.

- **Super-Li rich candidates:** A few super-Li rich stars have been reported in the literature exceeding the BBN value (e.g. the  $A(\text{Li}) = 2.87$  star in the globular cluster M4; Monaco et al. 2012). Other stars show abundances much above the meteoritic values of  $A(\text{Li}) = 3.25$  (Deliyannis et al. 2002; Koch et al. 2012; Adamów et al. 2012). Suggested enhancement scenarios including planetary ingestion, Hypernovae, and binary transfer (to cite only a few) presumably face challenges in accounting for such extreme levels of Li-enhancement (e.g. Monaco et al. 2012; Koch et al. 2012).

In our model, such high  $A(\text{Li})$  values result from spallation in the C layer. C-spallation would occur for a narrow window of time delay ( $8.3 \text{ days} < t_{\text{delay}} < 13 \text{ days}$  for our fiducial values) and only if enough  $> 0.42 \text{ GeV}$  neutrons make it past the O-layer; i.e. mainly in dsQNe with  $E_{\text{QN}} \geq 10 \text{ GeV}$  and with  $M_{\text{C,SN}} > 0.1M_{\text{O,SN}}$  (see discussion in §4.1). These stringent constraints suggest that super-Li candidates (i.e. Pop. II low-mass stars with  ${}^7\text{Li}$  spallated in the C-layer in our model) should be relatively rare compared to normal (i.e. with  $A(\text{Li}) \sim 2.2$  from O-spallation) candidates.

- **Interstellar  ${}^7\text{Li}$  abundance:** Howk et al. (2012) reported measurements of interstellar  ${}^7\text{Li}$  abundance of the Small Magellanic Cloud with values nearly equal to the BBN predictions. We speculate that the measured value may be a signature of a gas swept up by a dsQN with important C-spallation (see discussion above). Interestingly the  ${}^6\text{Li}/{}^7\text{Li}=0.13$  measured by Howk et al.



(2012) is very close to the value predicted by Ouyed (2013; see §5.3 and Fig. 8 in that paper). The high  ${}^6\text{Li}/{}^7\text{Li}$  values are expected in our model since  ${}^6\text{Li}$  and  ${}^7\text{Li}$  would be produced with nearly equal proportions from spallation.

## 5. DISCUSSION AND PREDICTIONS

Below we discuss some implications of our model followed by specific predictions:

- **Formation of Pop. II low-mass stars:** There are two models for the transition from Pop. III to Pop. II discussed in the literature: (i) Atomic fine-structure line cooling (Bromm & Loeb 2003) where Pop. III gas clouds cool down by the emission of radiation in de-exciting metals. This could in principle break up the large Pop. III clouds into cores that would eventually form Pop. II stars. In this model, low-mass star formation can occur in gas that is enriched beyond the critical abundances of  $[\text{C}/\text{H}]_{\text{crit}} \sim -3.5 \pm 0.1$  dex and  $[\text{O}/\text{H}]_{\text{crit}} \sim -3 \pm 0.2$  dex (or  $Z > Z_{\text{cr.}} \sim 10^{-3.5} Z_{\odot}$ ); (ii) Dust-induced fragmentation (e.g. Schneider et al. 2006a). Molecular gas clouds are cooled-down by transferring their heat to the surrounding dust. This cool-down fragments Pop. III molecular clouds into low-mass cores. The dust-cooling model predicts critical metallicity  $Z$  that is smaller by a factor of 10-100 than the one predicted in line cooling models.

The discovery of SDSS J102915+172927 (Caffau et al. 2011), an ultra metal-poor (UMP) star with  $[\text{Fe}/\text{H}] \sim -5$  (and with no excess of carbon) born from a cloud with  $Z < Z_{\text{cri.}}$  may be a challenge for the line cooling model and seems to rather support a fragmentation induced by dust-cooling (see discussion in Silvia et al. 2010 and Nozawa et al. 2012; see also Klessen et al. 2012).

Another possible mechanism is cloud fragmentation by the formation of high density regions (e.g. Greif et al. 2011 and references therein). In our model, QNe release highly dense and relativistic ejecta that can drive the surrounding cloud into compression. This cloud would be contaminated by dsQN products as well. This compression could eventually fragment the cloud into highly dense cores that turn into low-mass stars (e.g. Machida et al. 2005). An advantage of our model is that Fe-poor objects do not necessarily have low  $Z$ , since dsQNe with low  $t_{\text{delay}}$  lead to spallation reactions that destroy the Ni-layer but leave outer CO-rich layers intact. Furthermore, one can have the opposite situation where PopIII-SNII C and O are spalled but not inner-layer Ni remains intact.

Figure 12 compares relative abundances of stable isotopes in a pristine cloud swept up by a  $t_{\text{delay}} = 3.5$  days dsQN to measured values in SDSS J102915+172927. Both the  $E_{\text{QN}} = 5$  GeV and the  $E_{\text{QN}} = 10$  GeV simulations give very encouraging fits to measured abundances although our model overproduces  ${}^{48}\text{Ti}$ . As noted earlier, large abundances of Fluorine and Scandium are expected in our model since these rare nuclides are a natural outcome of spallation processes (see §6.2 in Ouyed 2013). The  ${}^7\text{Li}$  plotted is an upper limit. since at time

delays of  $t_{\text{delay}} < \sim 10$  days (i.e. for  $[\text{Fe}/\text{H}] < -3$ ), the the PopIII-SNII envelope temperature exceeds  $2.5 \times 10^6$  K which reduces the final abundance of spalled  ${}^7\text{Li}$ .

- **The primordial, Pop. III, IMF:** Our model requires no modification to the primordial IMF (the very massive  $35M_{\odot}$ - $200M_{\odot}$  Pop. III progenitors found in simulations; e.g. Wise&Abel 2007) and does not contradict observations that hint at contamination of Pop. II star-forming clouds by SNII metals, where these SNII progenitors were  $10M_{\odot}$ - $50M_{\odot}$  stars (e.g. Umeda&Nomoto 2005; Tumlinson et al. 2004). Without dsQNe, these observations contradict the primordial IMF, for the observations point at  $10M_{\odot}$ - $50M_{\odot}$  progenitors, and the primordial IMF postulates much more massive progenitors. However, we have argued in previous work that the dsQN can solve this apparent contradiction (see §6.3 in Ouyed 2013 for more discussion and relevant references).
- **The statistics:** In a heavy Pop. III IMF (e.g. see discussion in Larson 1998; see also Schneider et al. 2006b and references there in), dsQNe progenitors would contribute a small percentage of the population. Thus, according to our model, this scarcity of the resulting low-mass Pop. II stars in the galactic halo may be a reflection of the IMF of Pop. III stars (specifically the lower mass end of the distribution). Interestingly, the statistics of the known old,  $[\text{Fe}/\text{H}] < -2$  stars are rare in the Galaxy and represent only a small percentage of the total stellar mass (see Table 3 in Beers&Christlieb 2005).

In the QN model, a more massive progenitor NS leads to shorter time delays between the SN explosion and the QN explosion. The mass of a NS is likely to be proportional to the mass of its progenitor star, i.e. a massive core in a SNII explosion will experience a larger fall-back than a lighter core. The more massive the fall-back is, the faster will the NS acquire a critical density that would lead into quark de-confinement and thus the QN. Therefore, massive NSs will lead to short time delays. Because time delay is inversely proportional to the mass of the progenitor star, short  $t_{\text{delay}}$  dsQNe should be the rarest in a heavy Pop. III IMF, if the IMF peaks at  $\sim 40M_{\odot}$ . In other words, the lower the  $[\text{Fe}/\text{H}]$  (i.e. the shorter the  $t_{\text{delay}}$ ) the smaller the statistics of the ensuing Pop. II stars. In this picture, Hyper-Metal Poor (HMP) stars (with  $[\text{Fe}/\text{H}] < -5$  in the terminology of Beers&Christlieb 2005) would have originated in pristine clouds swept up by dsQNe from progenitors on the high end in the  $20M_{\odot} < M_{\text{prog.}} < 40M_{\odot}$  mass range. However, this conclusion relies heavily on the exact shape of the Pop. III IMF which remains to be confirmed.

- **Origin of HMP stars:** HMP stars show very peculiar abundance enhancements of C, N, and O. Astronomers have argued that these abundances may have been a consequence of binary mass transfers (Suda et al. 2004). This hypothesis awaits the discovery of radial velocity variations in HMP stars. Furthermore, this hypothesis implies that the stellar IMF at  $Z < 10^{-5}Z_{\odot}$  was biased towards intermediate mass stars (Tumlinson 2007). We argue that the enhanced abundance of C in HMP stars is not necessarily a consequence of bi-

rarity, but may be a signature of a dsQN. A dsQN with a sufficiently low  $t_{\text{delay}}$  would deplete its  $^{56}\text{Ni}$  layer but leave its C layer mostly intact. This would create a large ratio between C and Fe, which leads to an observed enhancement of C. In the binary accretion scenario, a large abundance of C should be accompanied by high levels of s-process which is not always observed (e.g. Cohen et al. 2006). In the dsQN model, slow neutrons capture processes and the resulting s-process products become important in dsQNe with  $t_{\text{delay}}$  leading to HMP stars (see §4 in Ouyed 2013 for more details; in particular eq. 11 in that paper).

We focus on two known HMP stars, HE0107-5240 ( $[\text{Fe}/\text{H}] = -5.54$ ; Christlieb et al. 2002) and HE1327-2326 ( $[\text{Fe}/\text{H}] = -5.76$ ; Frebel et al. 2008). These two stars have extremely high enhancements of the light elements C, N, and O relative to Fe. Figure 13 show a comparison of the peculiar chemical composition of HE 0107–5240 and HE 1327–2326 to abundances from dsQNe with for  $t_{\text{delay}} = 2.8$  days and  $t_{\text{delay}} = 2.6$  days, respectively. The measured relative abundances of elements,  $[X/\text{Fe}]$ , in these sources we take from Norris et al. (2013; see their Table 4). In our model, HMPs would be produced in a situation where QN neutrons are not energetic enough to traverse the inner Ni layer and spall C and O nuclei in the outer layers (see §3 in Ouyed 2013). This shielding of the outer CO layers combined with the substantial destruction of the  $^{56}\text{Ni}$  layer explains the large  $[\text{C}/\text{Fe}]$  and  $[\text{O}/\text{Fe}]$  in these objects (see Figures 1, 2 and 3). We find a good fit to measured abundances except for  $^{48}\text{Ti}$  which is overproduced in our model.

There is a strong apparent depletion of lithium, ( $A(\text{Li}) < 1.5$ ) in these two HMP stars. It's unlikely that HE1327-2326 depleted its own lithium through conventional means. A traditional mechanism for lowering the abundance of lithium would be photospheric depletion. In this picture, lithium is diffused under the photosphere and destroyed by high temperature protons. However, photospheric depletion for HE1327-2326 is improbable, given the star's light mass and low temperature of  $T_{\text{eff}} \sim 6000$  K. It's possible that HE0107-5240 may have destroyed some  $^7\text{Li}$  through photospheric depletion, but it seems unlikely that this process would lower the lithium abundance significantly below the plateau. Our model leads to the right levels of  $^7\text{Li}$  abundances, although the  $^7\text{Li}$  abundance from our simulations should be considered upper limits since  $[\text{Fe}/\text{H}] < -3$  for HMPs (see §4.1).

However, the extreme N abundance in HE1327-2326 can be better fit in our model if we assume  $^{14}\text{N}$  to be present in reasonable amounts in the PopIII-SNII ejecta. Interestingly, it has already been argued that  $^{14}\text{N}$  could be produced in Pop. III stars close to the  $\sim 40M_{\odot}$  limit (Heger&Woosley 2010); this limit is lower when taking rotation into account (Joggerst et al. 2010). In our proposed picture, the extreme  $[\text{C}/\text{Fe}]$  and  $[\text{O}/\text{Fe}]$  values in HE1327-2326 is already indicative of a dsQN progenitor with mass at the high end of the  $20M_{\odot} < M_{\text{prog.}} < 40M_{\odot}$  mass range. It is only fitting and natural to assume some  $^{14}\text{N}$  already present in the PopIII-SNII ejecta. Of course, our model does

not rule out the possibility of a companion at play in the case of HE1327-2326 given the initial CNO abundances we had to adopt for the fits.

### 5.1. Predictions

We now list some predictions of our model:

- Spallation reactions in dsQNe would chemically contaminate Pop. III clouds, and therefore affect the  ${}^6\text{Li}/{}^7\text{Li}$  ratio. A gas cloud processed by both astration and dsQNe (we assume the astration hypothesis is correct, refer to discussion in §4.3) would leave different chemical signatures in daughter, Pop. II stars than a cloud only processed by astration. This  ${}^6\text{Li}/{}^7\text{Li}$  ratio is affected because dsQN enhances  ${}^6\text{Li}$  abundance by spalling the O-layer. Therefore, the dsQNe-astration case should yield a larger  ${}^6\text{Li}/{}^7\text{Li}$  ratio than a dsQNe-deficient case, i.e. dsQNe-astration should produce  ${}^6\text{Li}/{}^7\text{Li} > 10^{-4}$ . Thus, we predict that two types of low-mass, Pop. II stars should be observed: a high  ${}^6\text{Li}/{}^7\text{Li}$  ratio star that was born from clouds that were processed by both dsQNe and astration, and a low  ${}^6\text{Li}/{}^7\text{Li} \sim 10^{-4}$  star produced by clouds that were only processed by astration.
- We found that dsQNe with  $8.3 \text{ days} < t_{\text{delay}} < 13 \text{ days}$  and  $E_{\text{QN}} \geq 10 \text{ GeV}$ , lead to spallation in the C-layer, which resulted in  ${}^7\text{Li}$  abundances exceeding meteoritic values ( $A(\text{Li}) \sim 3.25$ ). In these dsQNe, the destruction of C at the expense of lighter elements, means that super-Li rich low-mass stars should also show relative depletion in carbon. However,  ${}^{12}\text{C}$  is also a by-product of spallation in the  ${}^{16}\text{O}$  layer which suggest that not all super-Li candidates should appear carbon poor.
- QNe with  $t_{\text{delay}} < 2 \text{ days}$  would lead to excessive (almost complete) destruction of  ${}^{56}\text{Ni}$ . Thus, this QNe would lead to low-mass Pop. II stars with much lower  $[\text{Fe}/\text{H}]$  values than already observed HMP stars. These iron-poor stars should eventually be discovered if QNe with extremely short time delays occur in nature. However, these dsQNe are statistically extremely rare since they would originate from stars lying the closest to the black hole limit ( $\sim 40M_{\odot}$ ): i.e. dsQNe with massive enough NS to trigger quark de-confinement within a small  $t_{\text{delay}}$ .
- Pristine clouds swept up by dsQNe could produce low-mass Pop. II stars that have excessive CNO enhancements. Clouds processed by short-delayed ( $t_{\text{delay}} < 2.5 \text{ days}$  or  $[\text{Fe}/\text{H}] < -6$ ) dsQNe could produce these stars in binaries. In the dsQN scenario, original C and O (and N for the more massive dsQN progenitors) from SNII ejecta would be enhanced by spallation products. Furthermore, C, N, and O could be further enhanced by material accreted from the companion star. These CNO-enhanced objects should lead to  $[\text{C}/\text{Fe}]$ ,  $[\text{O}/\text{Fe}]$  and  $[\text{N}/\text{Fe}]$  values that are much greater than those measured so far in carbon-enhanced, extremely metal poor (CEMP) stars. The discovery of these CNO-enhanced stars, in particular if they show large  ${}^6\text{Li}/{}^7\text{Li}$  ratios and large

abundances of specific spallation products (e.g. Fluorine and Scandium, see Figures 1, 12 and 13), would strongly support our model - i.e. that the dsQN exists and it is crucial for understanding metal-poor Pop. II stars and the Spite plateau.

- We reiterate a previous point that the QN ejecta is not only neutron-rich, but rich in  $A > 130$  elements as well (Jaikumar et al. 2007; see discussion in §6.4 in Ouyed 2013). A typical QN ejects on average  $\sim 10^{-4}$ - $10^{-3}M_{\odot}$  of ejecta rich in  $A > 130$  elements. This ejecta's mass is 10-100 times larger than the ejected mass of heavy element in typical core-collapse SN ejecta. A SNII merely produces  $\sim 10^{-6}M_{\odot}$  in heavy elements (e.g. Woosley et al. 1994 and references therein). Since we estimate that on average QNe occur at a rate of 1 for every 100 core-collapse SNe (Leahy&Ouyed 2009; Ouyed et al. 2009a&b), contamination by QNe should be equally important if not more dominant. These elements should be detectable in environments around low-mass Pop. II stars if these environments were contaminated by dsQNe. A possible site for the QN  $A > 130$  tracers might be the ISM environment studied by Howk et al. (2012) in the Small Magellanic Cloud. In this environment, the super-Li  $A(Li)$  value and the high  ${}^6\text{Li}/{}^7\text{Li}$  measured, might be indicative of a dsQN with C-spallation imprint.
- In this work and in Ouyed (2013), we argued that extremely metal-poor Pop. II low-mass stars could have formed in pristine clouds swept up by primordial dsQNe. Furthermore, in Ouyed et al. 2009a we showed that primordial dsQNe provide enough ionizing photons to re-ionize the universe, and thus provide the  $\sim 0.1$  detected optical depth in the CMB by WMAP. Thus according to our model, the end of the epoch of re-ionization should also coincide with the epoch of formation of Pop. II low-mass stars. A notion which could be verified observationally.

## 6. CONCLUSION

In this paper we made a case for QNe (specifically dsQNe) as sources of  ${}^7\text{Li}$  in the pre-Galactic era. Lithium is produced by spallation on the PopIII-SNII ejecta material. For dsQNe with  $t_{\text{delay}} > t_{\text{outer}} \sim 8.3$  days, spallation in the Oxygen layer produces a  ${}^7\text{Li}$  plateau of  $A(Li) \sim 2.2$ , where this lithium abundance matches with observations of Spite&Spite (1982). We argue for a synergy between our model and the astration model of Piau et al. (2006). In the astration-dsQN scenario,  ${}^7\text{Li}$  that was produced in the big bang is first destroyed inside Population III stars of a 20-40 $M_{\odot}$  range. Some of these stars then turn into dsQNe and produce Spite abundances for lithium following spallation in the O-layer. In our model, instabilities in the pristine cloud swept-up by the SN+QN (i.e. dsQN) ejecta should lead to the formation of metal poor, low-mass stars. These stars have chemical abundances that compare well with the enhancements observed in old metal-poor dwarves. Moreover, abundances are compatible to the values observed in turn-off stars located in globular cluster. Furthermore, our model predicts that the most iron-poor stars likely formed from

gas clouds processed by low  $t_{\text{delay}}$  dsQNe. In this dsQNe picture, iron deficiency is not associated with age. In contrast to our picture, convention dictates that iron-content is proportional with cosmic age. This disentanglement between age and iron abundance calls for a paradigm shift in our understanding of iron-content in stars.

In today's universe, QNe should be associated with massive star ( $20\text{-}40M_{\odot}$ ) regions. At low redshift, dsQNe would manifest themselves as superluminous SNe (SLSNe)(Ouyed et al. 2002; Leahy&Ouyed 2008; Ouyed et al. 2010) with a distinct "double-hump" light-curve – the first hump correspond to the core-collapse SN explosion proper and the second hump to the re-energization of the SN shell by the QN (see Ouyed et al. 2009b; Ouyed&Leahy 2013). Ouyed et al. (2011). have suggested dsQNe signatures in the context of Ni-poor, Ti-rich SNe such as Cas A, and in the context of other peculiar SNe. Interestingly, the  $t_{\text{delay}}$  range used in the context of this paper is close to the  $t_{\text{delay}}$  range found in other dsQNe studies. The  $t_{\text{delay}}$  ranges explored in this paper compare favourably to fits used for SLSNe light-curves ( $2 \text{ days} < t_{\text{delay}} < 20 \text{ days}$ ) (e.g. Ouyed et al. 2012; Kostka et al. 2012), and dsQNe fits applied to chemically peculiar SNe (Ouyed et al. 2011). This similarity of  $t_{\text{delay}}$  ranges across QN studies may be a hint to a universal nature in the physics underlying the QN (or a self-consistency check). These ranges in  $t_{\text{delay}}$ , combined with the predicted QN's gravitational wave signatures (Staff et al. 2012), should lead to dsQN signatures in future gravitational wave detectors.

The existence of de-confined quark matter in the superdense interior of NSs is a key question that has drawn considerable attention over the past few decades. Our model postulates that this de-confinement not only exists, but triggers the most energetic explosions in the universe - the QNe. In this paper, we have shown that the Spite plateau is created by QNe, i.e. this plateau indicates that quark matter exists inside massive NSs. Our work on the Spite plateau points at interesting relationship between the QN and the early universe: e.g. not only have we explored the QN as a mechanism for the formulation of very low-metal Pop. II stars (Ouyed 2013 and this work) but other studies have explored the QNe as key to the universe's re-ionization (Ouyed et al. 2009a) as well. Other cosmological implications for the QN have been discussed as well (Ouyed&Staff (2013)).

I thank Jan Staff and Brian Niebergal for comments on the manuscript. I also thank Amir Ouyed for editing the manuscript. The research of R.O. is supported by an operating grant from the National Science and Engineering Research Council of Canada (NSERC).

## REFERENCES

- []Abel, T., Bryan, G. L., & Norman, M. L. 2002, *Science*, 295, 93
- []Adamów, M., Niedzielski, A., & Wolszczan, A. 2012, *Mem. S. A. It. Suppl.*, 22, 48
- []Albornoz Vásquez, D., Belikov, A., Coc, A., Silk, J., & Vangioni, E. 2012, *Phys. Rev. D*, 86, 063501
- []Angulo, C., Casarejos, E., Couder, M., et al. 2005, *ApJ*, 630, L105
- []Aoki, W., Honda, S., Beers, T. C., et al. 2007, *ApJ*, 660, 747
- []Arnett, D.W. 1996, *Supernovae and Nucleosynthesis*, Princeton Univ. Press. p. 188

- []Asplund, M., Lambert, D. L., Nissen, P. E., Primas, F., & Smith, V. V. 2006, *ApJ*, 644, 229
- []Beers T. C., Christlieb N., 2005, *Ann. Rev. A&A*, 43, 531
- []Bodmer, A.R. 1971, *Phys. Rev. D*, 4, 1601
- []Bonifacio, P., Molaro, P., Sivarani, T., et al. 2007, *A&A*, 462, 851
- []Bonifacio, P., Monaco, L., Sbordone, L., Villanova, S., & Pancino, E. 2010, *IAU Symposium*, 268, 269
- []Bromm, V., & Loeb, A., 2003, *Nature*, 425, 812
- []Bromm, V., & Larson, R. B. 2004, *ARA&A*, 42, 79
- []Caffau, E., Bonifacio, P., François, P., et al. 2011, *Nature*, 477, 67
- []Caughlan, G. R., & Fowler, W. A. 1972, *Nature Physical Science*, 238, 23
- []Cayrel, R., Depagne, E., Spite, M., et al. 2004, *A&A*, 416, 1117
- []Chaboyer, B., & Demarque, P. 1994, *ApJ*, 433, 510
- []Chakraborty N., Fields B. D., & Olive K. A., 2011, *Phys. Rev. D*, 83, 063006
- []Charbonnel, C., & Talon, S. 2005, *Science*, 309, 2189
- []Cherchneff, I., & Dwek, E. 2009, *ApJ*, 703, 642
- []Christlieb, N., Bessell, M. S., Beers, T. C., et al. 2002, *Nature*, 419, 904
- []Coc, A., Olive, K. A., Uzan, J.-P., & Vangioni, E. 2009, *Phys. Rev. D*, 79, 103512
- []Coc, A., & Vangioni, E. 2010, *J. Phys. Conf. Ser.*, 202, 012001
- []Cohen, J. G. et al. 2006, *AJ*, 132, 137
- []Cyburt, R. H., Fields, B. D., & Olive, K. A. 2004, *Phys. Rev. D*, 69, 123519
- []Cyburt, R. H., Fields, B. D., & Olive, K. A. 2008, *J. Cosmol. Astro-Part. Phys.*, 11, 12
- []Cyburt R. H., Ellis J., Fields B. D., Luo, F., Olive K. A., & Spanos V. C., 2010, *J. Cosmol. Astropart. Phys.*, 10, 32
- []Deliyannis, C. P., Demarque, P., & Kawaler, S. D. 1990, *ApJS*, 73, 21
- []Deliyannis, C. P., Steinhauer, A., & Jeffries, R. D. 2002, *ApJ*, 577, L39
- []Dunkley, J., Komatsu, E., Nolte, M. R., et al. 2009, *ApJS*, 180, 306
- []Fields, B. D. 2011, *Annual Review of Nuclear and Particle Science*, 61, 47
- []Frebel, A., Collet, R., Eriksson, K., Christlieb, N., & Aoki, W. 2008, *ApJ*, 684, 588
- []Greif, T. H., Springel, V., White, S. D. M., et al. 2011, *ApJ*, 737, 75
- []Heger, A., & Woosley, S. E. 2010, *ApJ*, 724, 341
- []Howk, J. C., Lehner, N., Fields, B. D. & Mathews, G. J. 2012, *Nature*, 489, 121
- []Iocco, F., Mangano, G., Miele, G., Pisanti, O., & Serpico, P. D. 2009, *Phys. Rep.*, 472, 1
- []Itoh, N. 1970, *Prog. Theor. Phys.*, 44, 291
- []Jaikumar, P., Meyer, B. S., Otsuki, K., & Ouyed, R. 2007, *A&A*, 471, 227
- []Jedamzik, K., Choi, K.-Y., Roszkowski, L., & Ruiz de Austri, R. 2006, *Journal of Cosmology and Astro-Particle Physics*, 7, 7
- []Jedamzik, K., & Pospelov, M. 2009, *New J. Phys.*, 11, 105028
- []Joggerst et al. 2010, *ApJ*, 709, 11
- []Keränen, P., Ouyed, R., & Jaikumar, P. 2005, *ApJ*, 618, 485
- []Klessen, R. S., Glover, S. C. O., & Clark, P. C. 2012, *MNRAS*, 421, 3217
- []Koch, A., Lind, K., Thompson, I. B., & Rich, R. M. 2012, *Mem. S. A. It. Suppl.*, 22, 79
- []Kohri, K., & Santoso, Y. 2009, *Phys. Rev. D*, 79, 043514
- []Kostka, M., Koning, N., Ouyed, R., Leahy, D., & Steffen, W. 2012, *arXiv:1206.7113*
- []Komatsu, E., Smith, K. M., Dunkley, J., et al. 2011, *ApJSuppl.*, 192, 18
- []Lambert, D. L. 2004, in *AIP Conf. Proc.* 743, *The New Cosmology*, ed. R. E. Allen, D. V. Nanopoulos, & C. N. Pope (New York: AIP), 206
- []Larson, R. B. 1998, *MNRAS*, 301, 569
- []Larson, D., Dunkley, J., Hinshaw, G., et al. 2011, *ApJ Supplement Series*, 192, 16
- []Leahy, D., & Ouyed, R. 2008, *MNRAS*, 387, 1193

- [Leahy, D., & Ouyed, R. 2009, *Advances in Astronomy*, 2009
- [Limongi, M., & Chieffi, A. 2012, *ApJ Supplement Series*, 199, 38
- [Loeb, A., Ferrara, A., & Ellis, R. S. 2008, *First Light in the Universe*, ed. Loeb, A., Ferrara, A., & Ellis, R. S.
- [Machida, M. V., Tomisaka, K., Nakamura, F., & Fujimoto, M. Y. 2005, *ApJ*, 622, 39
- [McCray R., 1985, in *Spectroscopy of Astrophysical Plasmas*, edited by A. Delgarno & D. Layzer, p. 270
- [McWilliam, A. 1997, *ARA&A*, 35, 503
- [Meléndez, J., & Ramírez, I. 2004, *ApJ*, 615, L33 (MR04)
- [Michaud, G., Fontaine, G., & Beaudet, G. 1984, *ApJ*, 282, 206
- [Monaco, L., Villanova, S., Bonifacio, P. et al. 2012, *A&A*, 539, A157
- [Mucciarelli A., Salaris M., Lovisi L., Ferraro F. R., Lanzoni B., Lucatello S., Gratton R. G., 2011, *MNRAS*, 412, 81
- [Nakamura, F. & Umemura, M. 2002, *ApJ*, 569, 549
- [Niebergal, B., Ouyed, R., & Jaikumar, P. 2010, *Phys. Rev. C*, 82, 062801
- [Nissen P.E., Akerman C., Asplund M., Fabbian D., Kerber F., Kaufl H.U., Pettini M., 2007, *A&A* 469, 319
- [Norris, J. E., Yong, D., Bessell, M. S., et al. 2013, *ApJ*, 762, 28
- [Nozawa, T., Kozasa, T., Umeda, H., Maeda, K., & Nomoto, K. 2003, *ApJ*, 598, 785
- [Nozawa, T., Kozasa, T., & Nomoto, K. 2012, *ApJ*, 756, L35
- [Ouyed, R., Dey, J., & Dey, M. 2002, *A&A*, 390, L39
- [Ouyed, R., Rapp, R., & Vogt, C. 2005, *ApJ*, 632, 1001
- [Ouyed, R., & Leahy, D. 2009, *ApJ*, 696, 562
- [Ouyed, R., Pudritz, R. E., & Jaikumar, P. 2009a, *ApJ*, 702, 1575
- [Ouyed, R., Leahy, D., & Jaikumar, P. 2009b, in *Proceedings for "Compact stars in the QCD phase diagram II (CSQCD II)"*, May 20-24, 2009, KIAA at Peking University, Beijing- P. R. China [arXiv:0911.5424]
- [Ouyed, R., Kostka, M., Koning, N., Leahy, D. A., & Steffen, W. 2012, *MNRAS*, 423, 1652
- [Ouyed, R. et al. 2011, *Physical Review Letters*, 107, 151103
- [Ouyed, R. 2013, *MNRAS*, 428, 236
- [Ouyed, R., & Staff, J. 2013, *Research in Astronomy and Astrophysics*, 13, 435
- [Ouyed, R., & Leahy, D. 2013, *Research in Astronomy and Astrophysics*, 13, 1202 [arXiv:1202.2400]
- [Piau L., Beers T. C., Balsara D. S., Sivarani T., Truran J. W., Ferguson J. W., 2006, *ApJ*, 653, 300
- [Piau, L. 2008, *ApJ*, 689, 1279
- [Pinsonneault, M. H., Deliyannis, C. P., & Demarque, P. 1992, *ApJS*, 78, 179
- [Pinsonneault, M. H., Steigman, G., Walker, T. P., & Narayanan, V. K. 2002, *ApJ*, 574, 398
- [Prantzos, N. 2007, *Space Sci. Rev.*, 130, 27
- [Ryan, S. G., Norris, J. E., & Beers, T. C. 1999, *ApJ*, 523, 654
- [Richard, O., Michaud, G., & Richer, J. 2005, *ApJ*, 619, 538
- [Salaris, M., & Weiss, A. 2001, *A&A*, 376, 955
- [Sbordone, L., Bonifacio, P., Caffau, E., et al. 2010, *A&A*, 522, A26
- [Sbordone, L., Bonifacio, P., & Caffau, E. 2012, *Mem. S.A.It.*, Vol. 75, 282
- [Schneider, R., Omukai, K., Inoue, A. K., & Ferrara, A. 2006a, *MNRAS*, 369, 1437
- [Schneider, R., Salvaterra, R., Ferrara, A., & Ciardi, B. 2006b, *MNRAS*, 369, 825
- [Shigeyama, T., & Tsujimoto, T. 1998, *ApJ*, 507, L135
- [Silvia, D. W., Smith, B. D., & Shull, J. M. 2010, *ApJ*, 715, 1575
- [Spite, F., & Spite, M. 1982, *A&A*, 115, 357



- []Spite, M., Cayrel, R., Plez, B., et al. 2005, *A&A*, 430, 655
- []Spite, M., Caffau, E., Andrievsky, S. M., Korotin, S. A. et al. 2011, *A&A* 528, A9
- []Spite, M., Spite, F., & Bonifacio, P. 2012, *Memorie della Societa Astronomica Italiana Supplementi*, 22, 9
- []Staff, J. E., Ouyed, R., & Jaikumar, P. 2006, *ApJ*, 645, L145
- []Staff, J. E., Jaikumar, P., Chan, V., & Ouyed, R. 2012, *ApJ*, 751, 24
- []Suda, T., Aikawa, M., Machida, M. N., Fujimoto, M. Y., & Iben, I., Jr. 2004, *ApJ*, 611, 476
- []Talon, S., Kumar, P., & Zahn, J.-P. 2002, *ApJ*, 574, L175
- []Talon, S., & Charbonnel, C. 2004, *A&A*, 418, 1051
- []Terazawa, H., 1979, INS-Report-338, University of Tokyo
- []Tumlinson, J., Venkatesan, A., & Shull, J. M. 2004, *ApJ*, 612, 602
- []Tumlinson, J. 2007, *ApJ*, 665, 1361
- []Umeda, H. & Nomoto, K. 2002, *ApJ*, 565, 385
- []Umeda, H., & Nomoto, K. 2005, *ApJ*, 619, 427
- []Vauclair, S. 1988, *ApJ*, 335, 971
- []Vogt, C., Rapp, R., & Ouyed, R. 2004, *Nuc. Phys. A*, 735, 543
- []Wise, J. H., & Abel, T. 2007, *ApJ*, 671, 1559
- []Witten, E. 1984, *Phys. Rev. D*, 30, 272
- []Woodsley, S. E., Wilson, J. R., Mathews, G. J., Hoffman, R. D., & Meyer, B. S. 1994, *ApJ*, 433, 229

TABLE 1

AVERAGE MULTIPLICITY ( $\zeta$ ) AND ENERGY OF SPALLATED NEUTRONS FOR DSQNE WITH  $T_{\text{DELAY}} = T_{\text{OUTER}} \sim 8.3$  DAYS; THIS IS THE REGIME WHERE THE QN NEUTRONS INTERACT WITH THE INNERMOST LAYERS ( $^{56}\text{Ni}$ ,  $^{32}\text{S}$ ,  $^{28}\text{Si}$ ). FOR THIS TIME DELAY,  $N_{\text{MFP},A_T} \sim 1$  WHICH MEANS THAT THE THICKNESS OF EACH TARGET LAYER IS EQUIVALENT TO ROUGHLY ONE SPALLATION MFP (SEE EQ. ??). SPALLATION STOPS AT THE  $^{28}\text{Si}$  LAYER SINCE THE SUBSEQUENT GENERATION OF NEUTRONS EXIT THE  $^{32}\text{S}$  LAYER WITH ENERGIES  $\sim 0.15$  GEV WHICH IS BELOW CRITICAL FOR SPALLATION TO ENSUE IN THE OVERLAYING LAYERS  $^{24}\text{Mg}$  LAYER ( $E_{\text{SP},\text{MG}} \sim 0.18$  GEV; SEE DISCUSSION FOLLOWING EQ. ??).

$A_T$	Primaries ( $E_0 = E_{\text{QN}} = 10$ GeV)			Primaries ( $E_0 = E_{\text{QN}} = 5$ GeV)		
	$^{56}\text{Ni}$	$^{32}\text{S}$	$^{28}\text{Si}$	$^{56}\text{Ni}$	$^{32}\text{S}$	$^{28}\text{Si}$
$\zeta_{\text{av},i}$	$\sim 13.1$	$\sim 3.6$	$\sim 1.4$	$\sim 11.3$	$\sim 2.8$	$\sim 1.1$
$E_{\text{av},i} = \frac{E_{\text{av},i-1}}{\zeta_{\text{av},i}}$ (GeV)	$\sim 0.77$	$\sim 0.21$	$\sim 0.15$	$\sim 0.44$	$\sim 0.16$	$\sim 0.15$
$^\dagger A_{\text{peak},i} \simeq A_T - \zeta_{\text{av},i}$	$\sim ^{44}\text{Ti}$	$\sim ^{28}\text{Si}$	$\sim ^{27}\text{Al}$	$\sim ^{45}\text{Sc}$	$\sim ^{28}\text{Si}$	$\sim ^{27}\text{Al}$
$^\ddagger \zeta_{\text{net},i} = \zeta_{\text{av},i-1} \times \zeta_{\text{av},i}$	$\sim 13.1$	$\sim 47.2$	$\sim 66$	$\sim 11.3$	$\sim 31.7$	$\sim 34.8$

$^\dagger$ The resulting spallation products would acquire a normal distribution peaking at atomic weight  $A_{\text{peak},i} \sim A_T - \zeta_i$ .

$^\ddagger$  The net multiplicity ( $\zeta_{\text{net}}$ ; see eq. 4 in Ouyed 2013) translates to a total spallation neutrons and protons which amounts to  $M_{\text{n+p}} = \zeta_{\text{net}} M_{\text{QN}} \sim 0.05\text{-}0.1 M_\odot$ .

TABLE 2: Average multiplicity ( $\zeta$ ) and energy of spallated neutrons in the oxygen ( $^{16}\text{O}$ ) layer for dsQNe with  $t_{\text{delay}} > t_{\text{outer}}$  (here  $t_{\text{delay}} = 12$  days); this is regime where the QN neutrons barely interact with the inner layers and proceed directly to the oxygen layer. The thickness of the oxygen layer (with  $M_{\text{O,SN}} = 1.5M_{\odot}$ ) is equivalent to  $N_{\text{sp.,O}} \sim 10$  sub-layers each of radial thickness or the order of a spallation mfp (see eq. 1). Spallation in the oxygen layer ceases when the neutron energy is below the threshold value for O-spallation ( $E_{\text{sp.,O}} \approx 0.27$  GeV) or when the neutrons run out of target material (i.e. after  $N_{\text{sp.,O}} \sim 10$  mfps).

$A_T = 16$	Primaries ( $E_0 = E_{\text{QN}} = 10$ GeV)					Primaries ( $E_0 = E_{\text{QN}} = 5$ GeV)				
	mfp 1	mfp 2	mfp 3	mfp 4	mfp 5	mfp 1	mfp 2	mfp 3	mfp 4	mfp 5
$\zeta_{\text{av.,i}}$	$\sim 3.8$	$\sim 2.7$	$\sim 2$	$\sim 1.5$	$\sim 1.1$	$\sim 3.2$	$\sim 2.4$	$\sim 1.7$	$\sim 1.3$	$\sim 1.1$
$E_{\text{av.,i}} = \frac{E_{\text{av.,i-1}}}{\zeta_{\text{av.,i}}} \text{ (GeV)}$	$\sim 2.7$	$\sim 1.0$	$\sim 0.5$	$\sim 0.34$	$\sim 0.28$	$\sim 1.6$	$\sim 0.7$	$\sim 0.4$	$\sim 0.3$	$\sim 0.28$
$^\dagger A_{\text{peak,i}} \approx 16 - \zeta_{\text{av.,i}}$	$^{12}\text{C}$	$^{13}\text{C}$	$^{14}\text{N}$	$^{14}\text{N}$	$^{15}\text{O}$	$^{13}\text{C}$	$^{14}\text{N}$	$^{14}\text{N}$	$^{15}\text{O}$	$^{15}\text{O}$
$^\ddagger \zeta_{\text{net,i}} = \zeta_{i-1} \times \zeta_i$	$\sim 3.8$	$\sim 10.3$	$\sim 20.6$	$\sim 31$	$\sim 34$	$\sim 3.2$	$\sim 7.7$	$\sim 13$	$\sim 17$	$\sim 19$

$^\dagger$ The resulting spallation products would acquire a normal distribution peaking at atomic weight  $A_{\text{peak,i}} \sim 16 - \zeta_i$ .

$^\ddagger$  The net multiplicity ( $\zeta_{\text{net}}$ ; see eq. 4 in Ouyed 2013) translates to a total spallation neutrons and protons which amounts to  $M_{\text{n+p}} = \zeta_{\text{net}} M_{\text{QN}} \sim 0.02$ - $0.04 M_{\odot}$ .

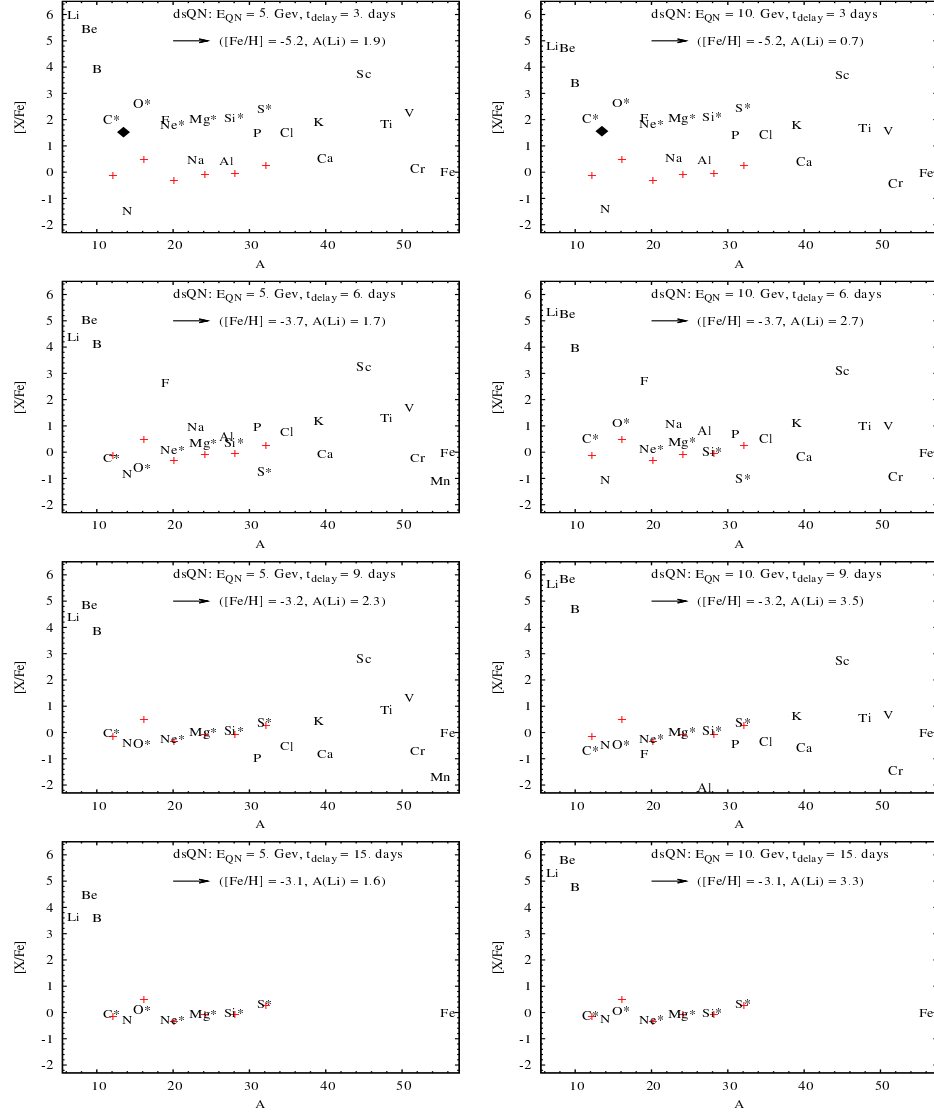


Fig. 1. Relative abundances  $[X/Fe]$  for spallation (sub-Fe) products versus mass number  $A$  ( $7 \leq A < 56$ ; only stable isotopes are shown here and in other figures in this paper) for a dsQN with 5 GeV (left panels) and 10 GeV (right panels) QN neutrons. Letters show abundances from our simulations with the CN enhanced nitrogen (for short  $t_{\text{delay}}$ ) shown as a filled diamond. The panels from top to bottom are for  $t_{\text{delay}}$ (days) = 3, 6, 9, 15, respectively. Also shown are the resulting  $[Fe/H]$  and  ${}^7\text{Li}$  abundance,  $A(\text{Li})$ . The plus signs represents the initial relative abundance of the original PopIII-SNII elements; these elements are identified by an asterisk (next to their names) as they evolve with  $t_{\text{delay}}$ . Their initial abundances in mass are  $M_{\text{Ni},\text{SN}} = 0.1M_{\odot}$ ,  $M_{\text{S},\text{SN}} = M_{\text{Si},\text{SN}} = M_{\text{Mg},\text{SN}} = M_{\text{Ne},\text{SN}} = 0.05M_{\odot}$ ,  $M_{\text{O},\text{SN}} = 1.5M_{\odot}$  and  $M_{\text{C},\text{SN}} = 0.15M_{\odot}$ . These initial abundances are the same in all of the figures in this paper unless stated otherwise. Similarly, unless stated otherwise, the mass of the cloud swept by a dsQN is set to  $M_{\text{sw}} = 10^5 M_{\odot}$  in all of our simulations.

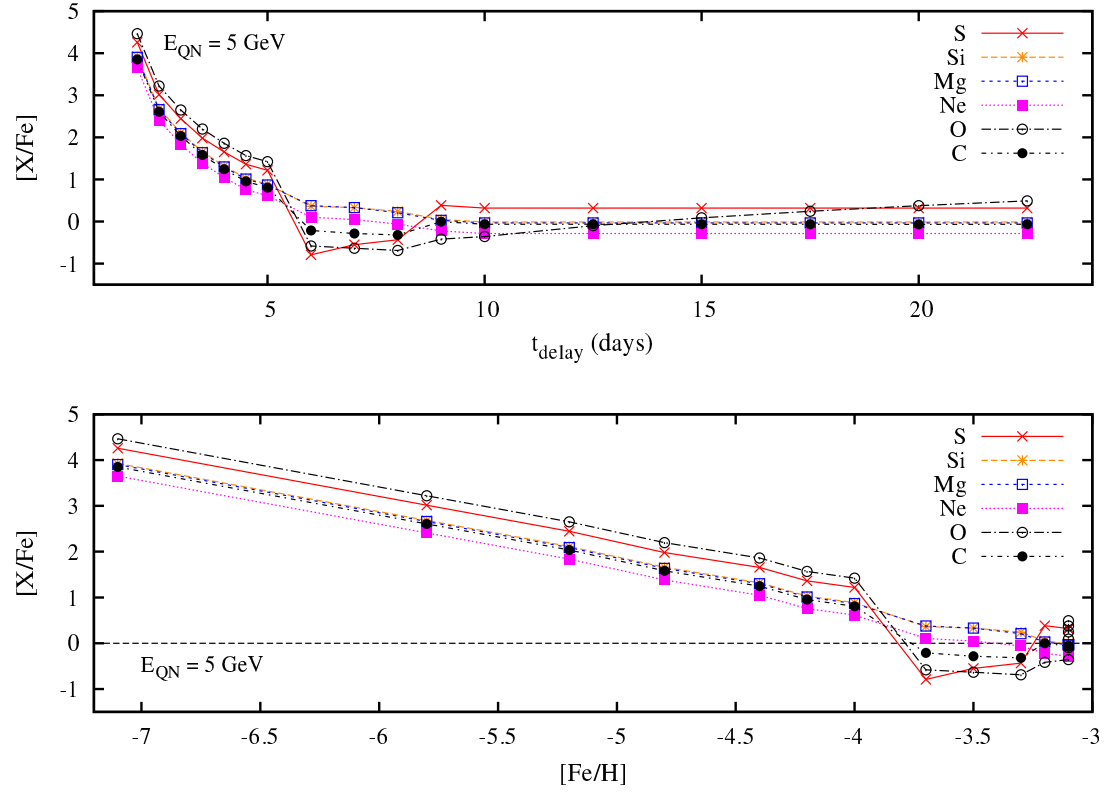
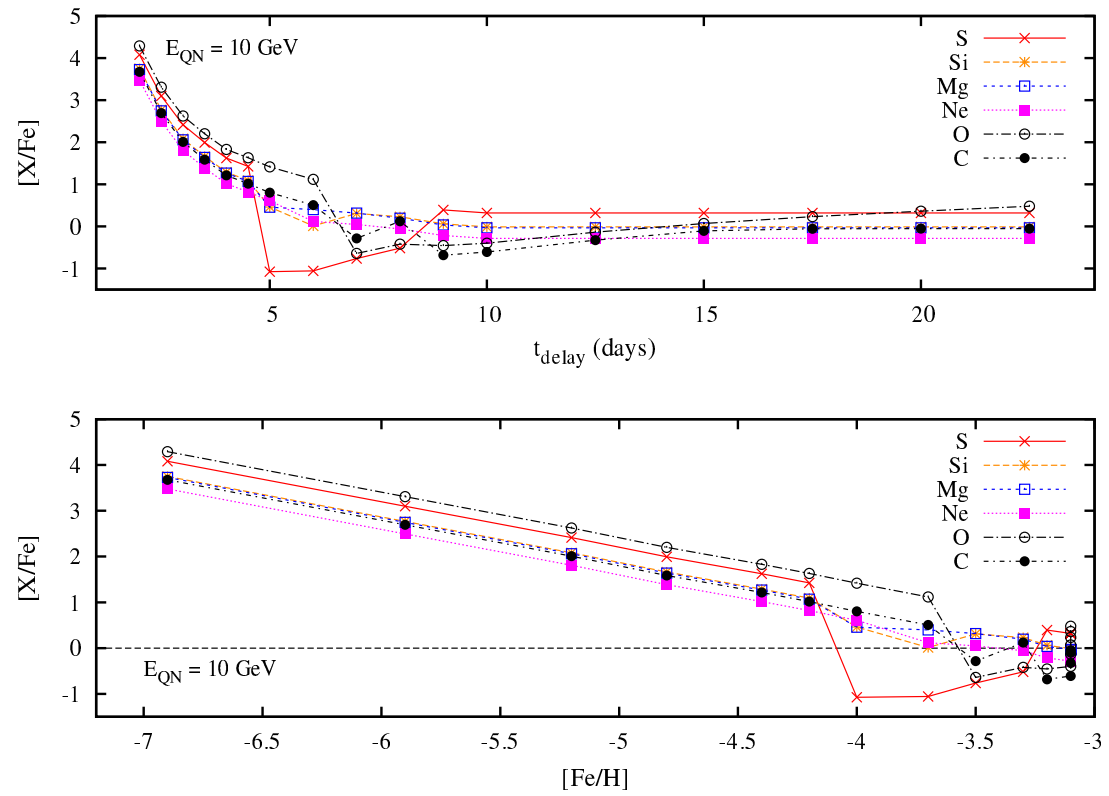


Fig. 2: Relative abundances  $[X/Fe]$  versus  $t_{\text{delay}}$  (top panel) and versus the corresponding  $[Fe/H]$  (bottom panel) for  $^{32}\text{S}$ ,  $^{28}\text{Si}$ ,  $^{24}\text{Mg}$ ,  $^{20}\text{Ne}$ ,  $^{16}\text{O}$  and  $^{12}\text{C}$  with initial relative abundances  $[X/Fe]_{X,\text{SN}} = 0.32, -0.01, -0.03, -0.28, 0.53, -0.09$ , respectively. These elements represent the original composition of the PopIII-SNII ejecta (i.e. the target material) in our model. Here,  $E_{QN} = 5 \text{ GeV}$ . The horizontal dashed line in the bottom panel corresponds to  $[X/Fe]=0$ .

Fig. 3: Same as in figure 2 but for  $E_{\text{QN}} = 10 \text{ GeV}$ .

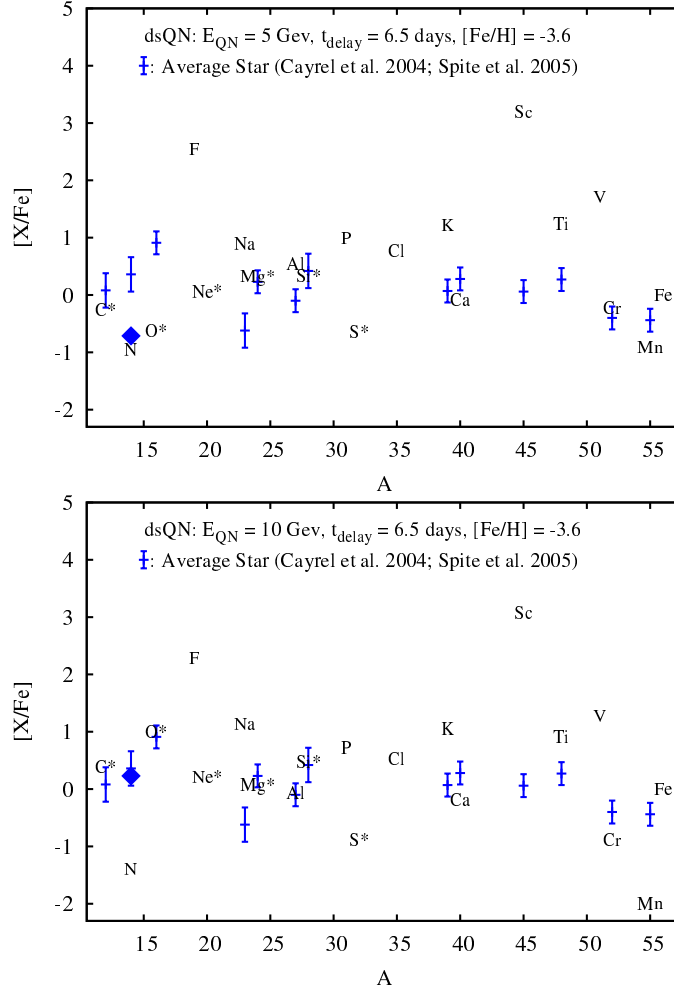


Fig. 4. Relative abundances  $[X/Fe]$  of sub-Fe spallation products (elements identified by their names) versus mass number  $A$  from simulations with  $t_{\text{delay}} = 6.5$  days; this resulted in  $[Fe/H] \approx -3.6$ . The CN enhanced nitrogen is shown by the filled diamond. Measured abundances of an average halo star (Cayrel et al. 2004; Spite et al. 2005) are also shown as plus (+) signs, with corresponding uncertainties, for a comparison. Top and bottom panels are for QN neutrons with  $E_{QN} = 5$  GeV and 10 GeV, respectively.

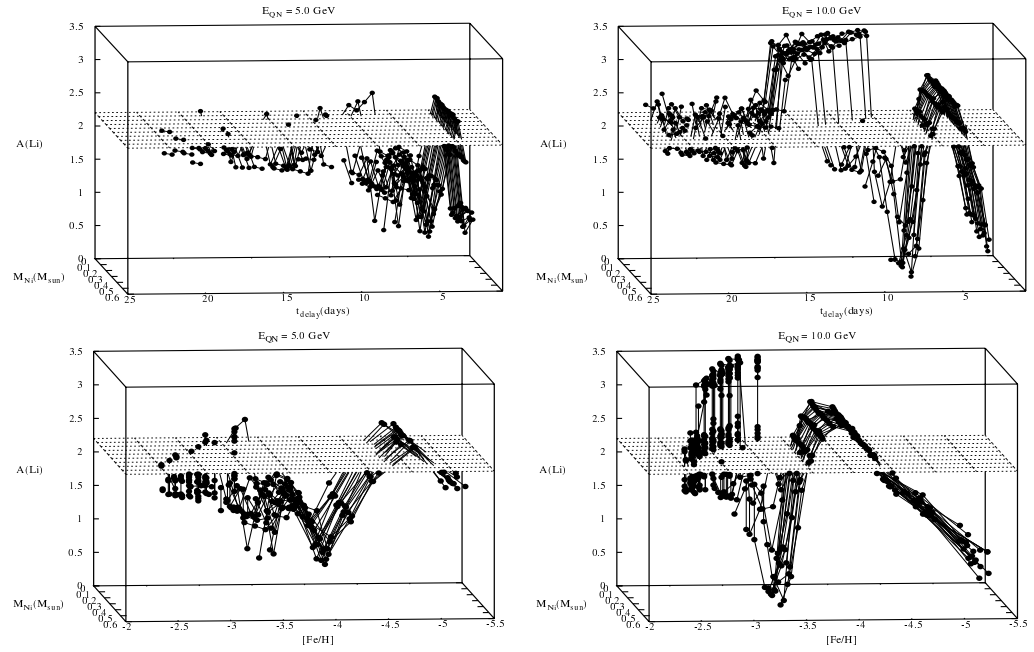


Fig. 5. Top panels:  $A(\text{Li})$  versus time delay ( $2 \text{ days} \leq t_{\text{delay}} \leq 30 \text{ days}$ ) and PopIII-SNII initial  $^{56}\text{Ni}$  mass ( $0.1M_{\odot} \leq M_{\text{Ni},\text{SN}} \leq 0.5M_{\odot}$ ). Bottom panels: The corresponding  $A(\text{Li})$  versus  $[\text{Fe}/\text{H}]$  ( $-7.5 < [\text{Fe}/\text{H}] < -2.5$ ; see 3.2.1). Left-hand and right-hand panels are for  $E_{\text{QN}} = 5 \text{ GeV}$  and  $10 \text{ GeV}$ , respectively. The horizontal plane corresponds to  $A(\text{Li}) = 2.2$ .



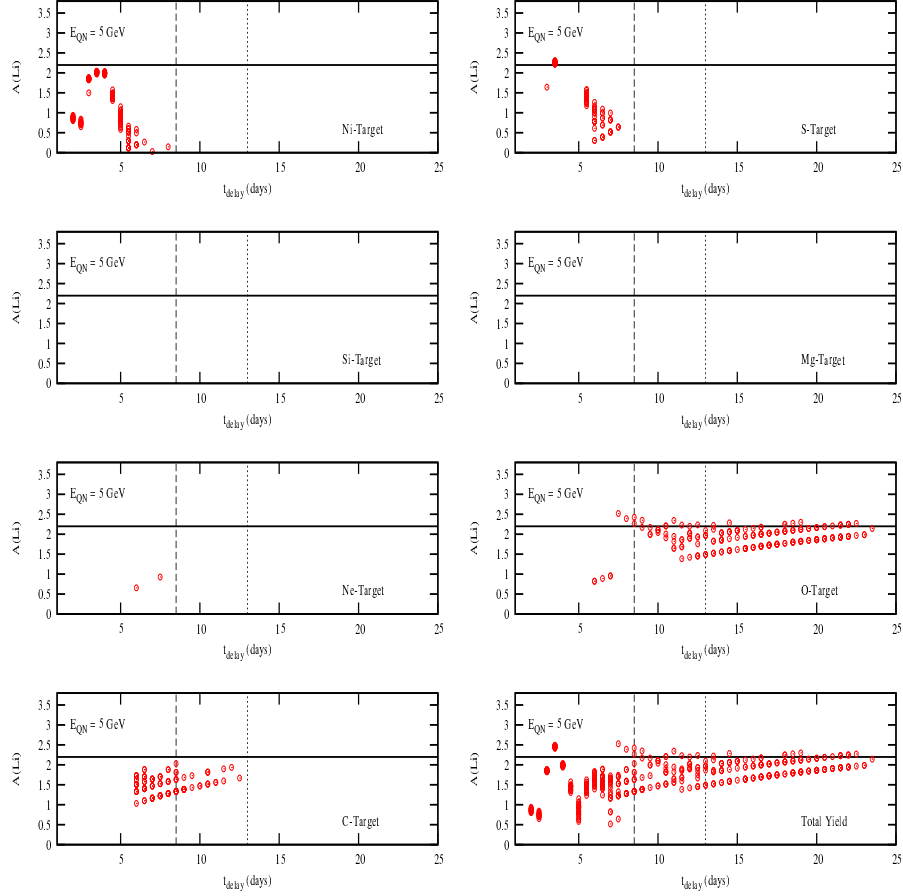


Fig. 6. The open circles show  $A(Li)$  versus  $t_{\text{delay}}$  per spallation target (Ni, S, Si, Mg, Ne, O and C) for the simulations shown in the left panels in figure 5 (i.e. for  $E_{QN} = 5$  GeV). The "Total Yield" panel shows  $A(Li)$  from all targets combined. The Horizontal lines corresponds to  $A(Li) = 2.2$ . The vertical dashed line shows  $t_{\text{outer}} \sim 8.3$  days while the dotted vertical line is at 13 days which defines the  $\Delta R_C = \lambda_{\text{sp,C}}$  limit (i.e.  $N_{\text{mf},C} = 1$ ) above which no spallation occurs in the C layer.

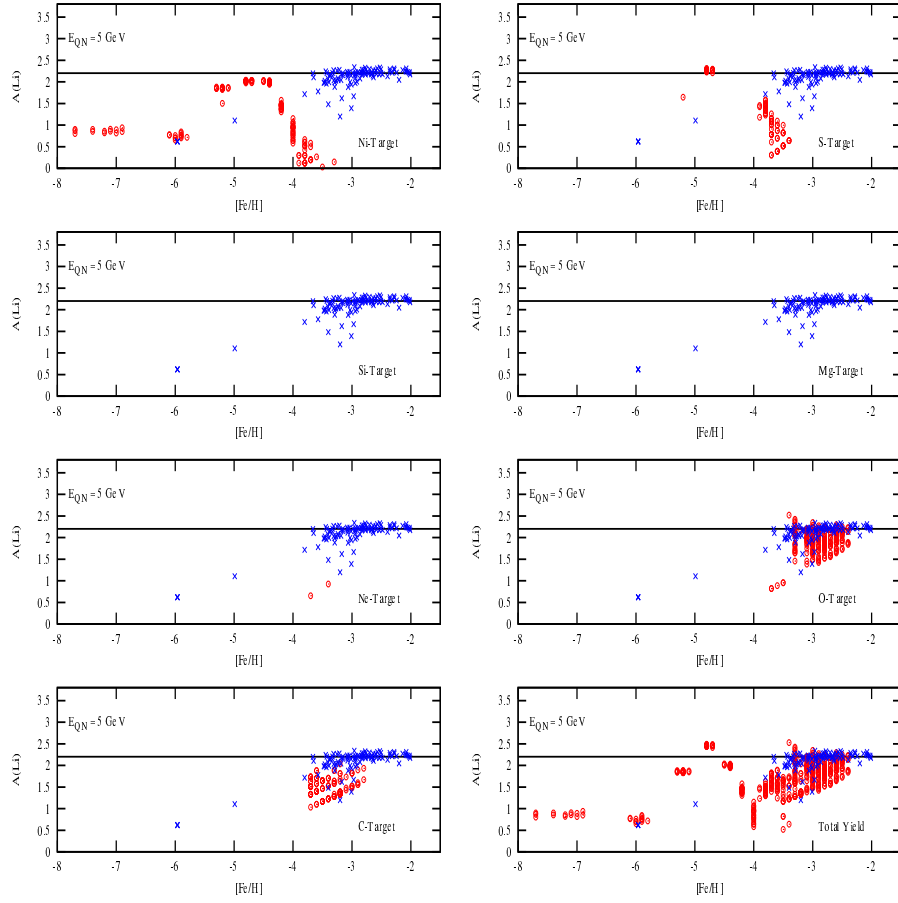


Fig. 7. The open circles show  $A(Li)$  versus  $[Fe/H]$  per spallation target (Ni, S, Si, Mg, Ne, O and C) for the simulations shown in the left panels in figure 5 (i.e. for  $E_{QN} = 5$  GeV). The crosses are measured  ${}^7Li$  abundances in halo and turn-off stars from Sbordone et al. (2012; see their figure 1 for references).

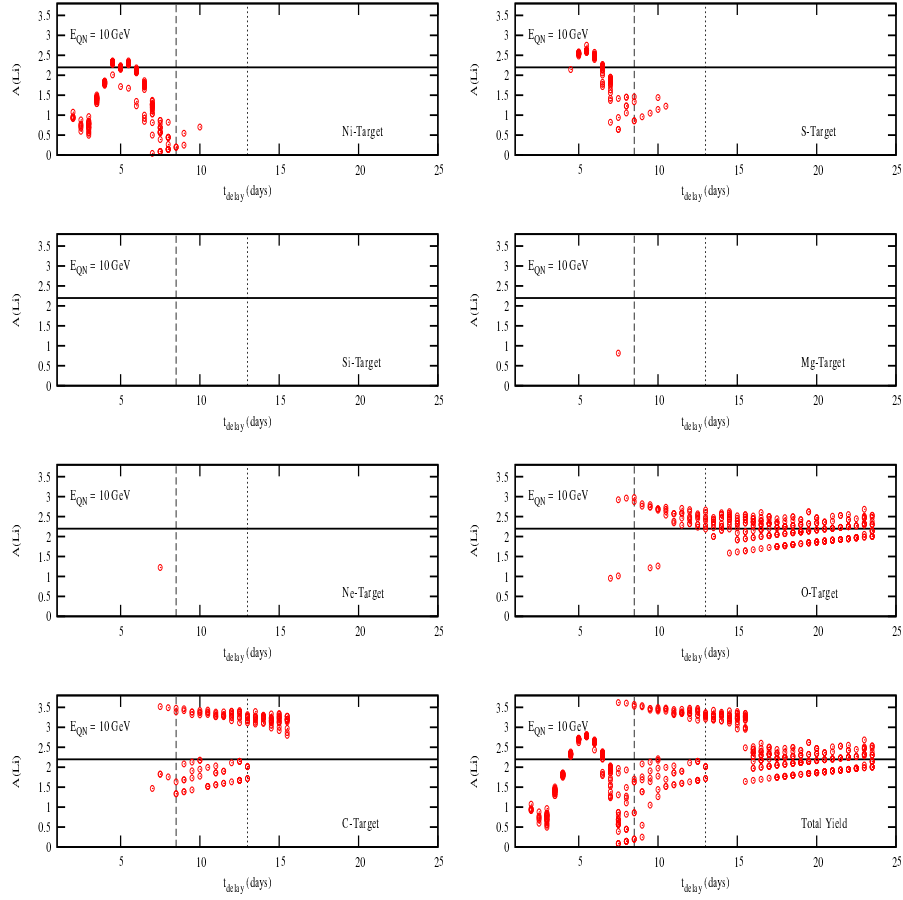


Fig. 8. Same as in figure 6 but for the  $E_{QN} = 10$  GeV simulations.

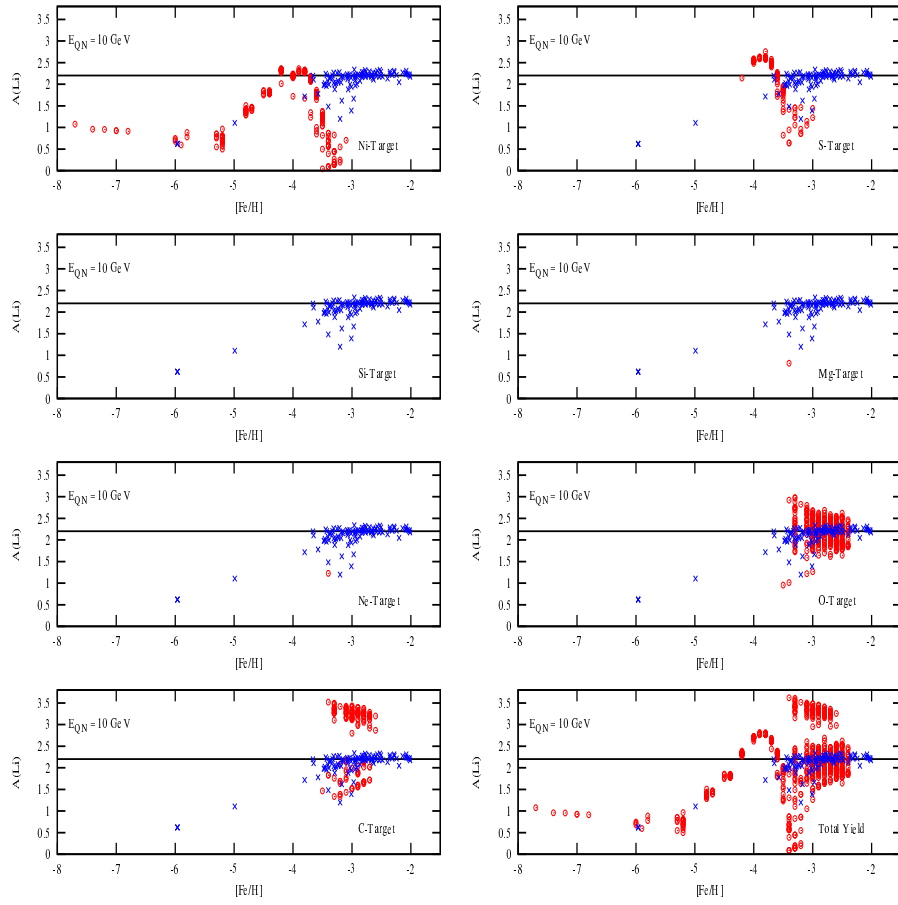


Fig. 9. Same as in figure 7 but for the  $E_{QN} = 10$  GeV simulations.

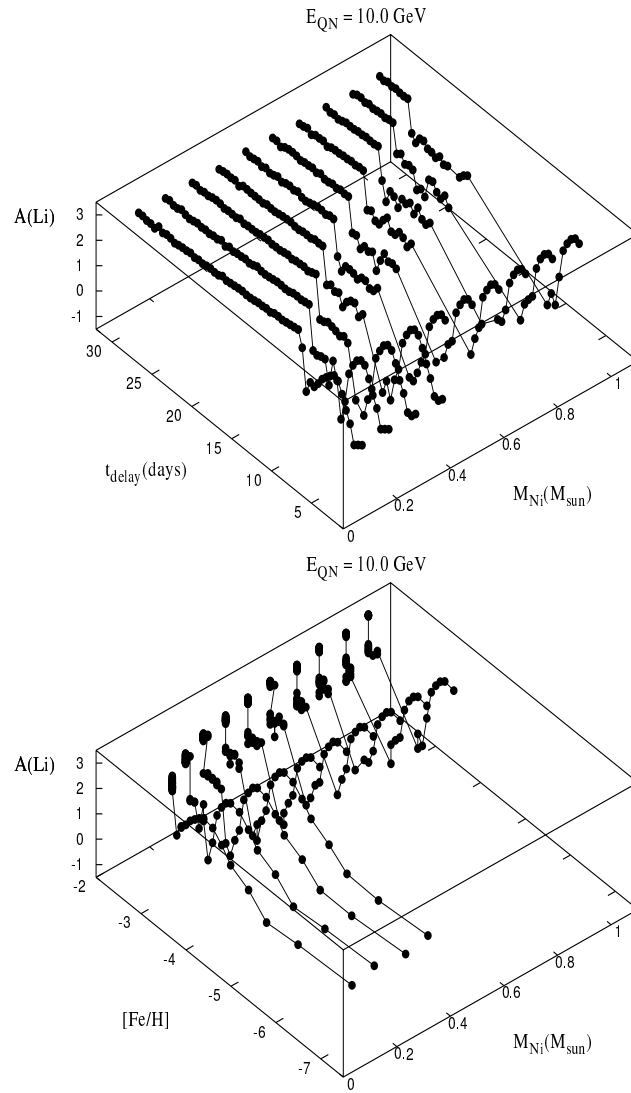


Fig. 10. Same as in figure 5 but for  $M_{C,SN} = M_{O,SN} = 1.5 M_{\odot}$ .

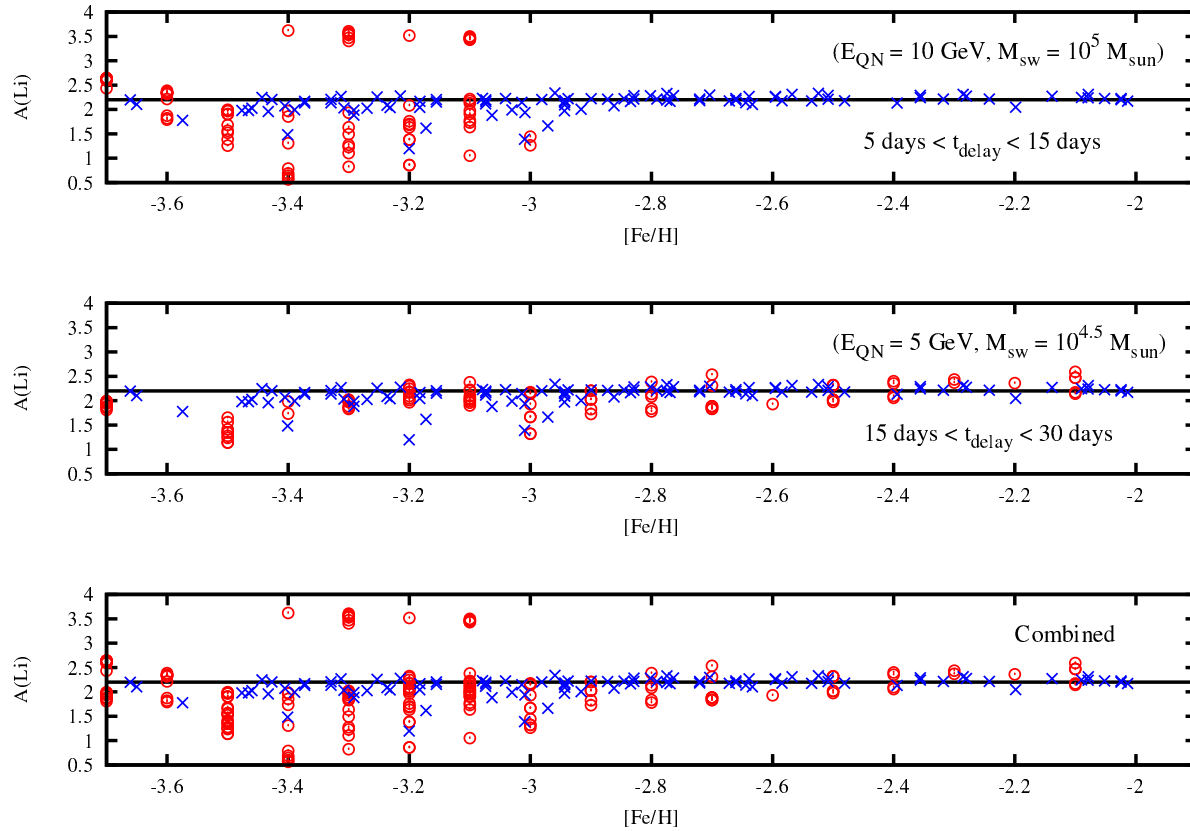


Fig. 11: Top panel:  $A(\text{Li})$  versus  $[\text{Fe}/\text{H}]$  for simulations with  $E_{\text{QN}} = 10 \text{ GeV}$ ,  $M_{\text{sw}} = 10^5 M_{\odot}$  and for  $5 \text{ days} < t_{\text{delay}} < 15 \text{ days}$ . Middle panel:  $A(\text{Li})$  versus  $[\text{Fe}/\text{H}]$  for simulations with  $E_{\text{QN}} = 5 \text{ GeV}$ ,  $M_{\text{sw}} = 10^{4.5} M_{\odot}$  and for  $15 \text{ days} < t_{\text{delay}} < 30 \text{ days}$ . Bottom panel:  $A(\text{Li})$  versus  $[\text{Fe}/\text{H}]$  resulting from all simulations for a range in  ${}^{56}\text{Ni}$  content,  $0.05 M_{\odot} \leq M_{\text{Ni,SN}} \leq 0.5 M_{\odot}$ . The crosses are measured  ${}^7\text{Li}$  abundances in halo stars and turn-off stars as described in Sbordone et al. (2012; see their figure 1 for the sources of the data). The Horizontal line corresponds to  $A(\text{Li}) \sim 2.2$ .

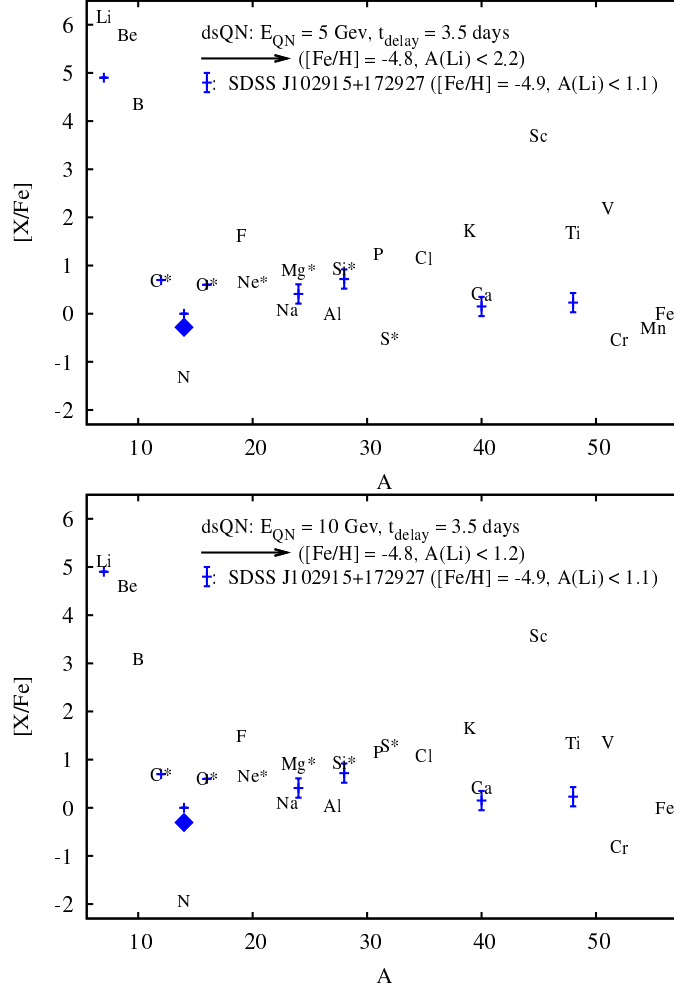


Fig. 12. Relative abundances  $[X/Fe]$  of sub-Fe spallation products (elements identified by their names) versus mass number  $A$  from simulations with  $t_{\text{delay}} = 3.5$  days which resulted in  $[Fe/H] \approx -4.8$ . The CN enhanced nitrogen is shown by the filled diamond. Top and bottom panels are for QN neutrons with  $E_{\text{QN}} = 5$  GeV and 10 GeV, respectively. SDSS J102915+172927's measured abundances are also shown, as plus (+) signs with the corresponding uncertainties, for a comparison (plus signs with no error bars are upper limits). We adopted measured abundances given in Caffau et al. (2011; see their Table 1) with an assumed upper limit for oxygen of  $[O/Fe] \sim 0.6$ . Best fits were found for initial abundances in mass of  $M_{\text{Ni},\text{SN}} = 0.1M_{\odot}$ ,  $M_{\text{S},\text{SN}} = M_{\text{Si},\text{SN}} = M_{\text{Mg},\text{SN}} = M_{\text{Ne},\text{SN}} = 0.01M_{\odot}$ ,  $M_{\text{O},\text{SN}} = 0.04M_{\odot}$  and  $M_{\text{C},\text{SN}} = 0.02M_{\odot}$ . The mass of the cloud swept by a dsQN was kept at  $M_{\text{sw}} = 10^5 M_{\odot}$ .

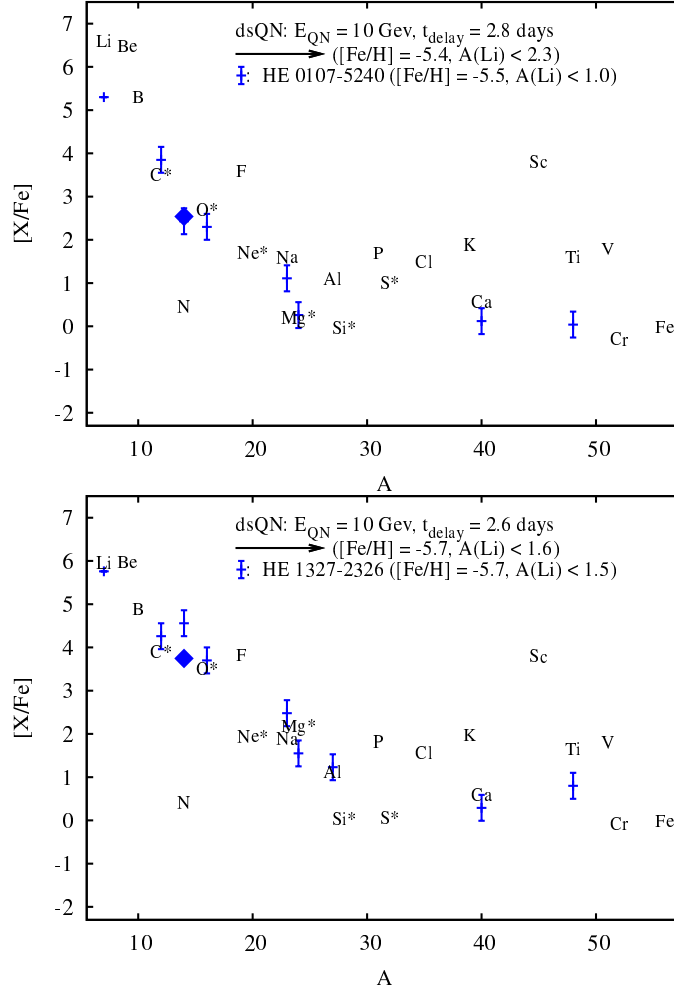


Fig. 13. **Top panel:** Relative abundances  $[X/Fe]$  of sub-Fe spallation products (elements identified by their names) versus mass number  $A$  from simulations with  $t_{\text{delay}} = 2.8$  days and  $E_{\text{QN}} = 10$  GeV which resulted in  $[Fe/H] \approx -5.4$  and  $A(Li) < 2.3$ . The CN enhanced nitrogen is shown by the filled diamond. HMP-HE-0107-5240's measured abundances are also shown, as plus (+) signs with the corresponding uncertainties, for a comparison (plus signs with no error bars are upper limits). The fit was found for initial abundances in mass of  $M_{\text{Ni},\text{SN}} = M_{\text{S},\text{SN}} = M_{\text{Si},\text{SN}} = 0.01M_{\odot}$ ,  $M_{\text{Mg},\text{SN}} = M_{\text{Ne},\text{SN}} = 0.02M_{\odot}$ ,  $M_{\text{O},\text{SN}} = 1.0M_{\odot}$  and  $M_{\text{C},\text{SN}} = 3.0M_{\odot}$ . The CN enhanced nitrogen was obtained for a 1% enhancement factor; **Bottom panel:** Relative abundances  $[X/Fe]$  of sub-Fe spallation products (elements identified by their names) versus mass number  $A$  from simulations with  $t_{\text{delay}} = 2.6$  days and  $E_{\text{QN}} = 10$  GeV which resulted in  $[Fe/H] \approx -5.7$  and  $A(Li) < 1.5$ . HMP-HE-0107-5240's measured abundances are also shown, as plus (+) signs with the corresponding uncertainties, for a comparison. The fit was found for initial abundances in mass of  $M_{\text{Ni},\text{SN}} = M_{\text{S},\text{SN}} = M_{\text{Si},\text{SN}} = 0.01M_{\odot}$ ,  $M_{\text{Mg},\text{SN}} = M_{\text{Ne},\text{SN}} = 0.02M_{\odot}$ ,  $M_{\text{O},\text{SN}} = 3.5M_{\odot}$  and  $M_{\text{C},\text{SN}} = 3.5M_{\odot}$ . Both cases were run for an  $M_{\text{sw}} = 10^5 M_{\odot}$  cloud swept by the dsQN. The measured abundances were taken from Norris et al. (2013).